NASA Technical Memorandum 85853

NASA TM-85853

NASA-TM-85853 19840003188

Stress-Corrosion Behavior of Aluminum-Lithium Alloys in Aqueous Salt Environments

P. P. Pizzo, R. P. Galvin and Howard G. Nelson

October 1983

NASA
National Aeronautics and
Space Administration

STRESS-CORROSION BEHAVIOR OF ALUMINUM-LITHIUM ALLOYS

IN AQUEOUS SALT ENVIRONMENTS

P. P. Pizzo

San Jose State University
San Jose, California 95192, U.S.A.

R. P. Galvin and Howard G. Nelson

NASA Ames Research Center
Moffett Field, California 94035, U.S.A.

The stress-corrosion susceptibility of two powder-metallurgy (P/M) alloys, Al-Li-Cu and Al-Li-Cu-Mg; two mechanically attrited (M/A) alloys, Al-Li-Cu and Al-Li-Mg; and two wrought, ingot alloys, X-2020 and AA7475, are compared. Time-dependent fracture in an aqueous sodium chloride environment under alternate-immersion condition was found to vary significantly between alloys. The stress-corrosion behavior of the two powder-metallurgy processed alloys was studied in detail under conditions of crack initiation, static crack growth, and fatigue-crack growth. A variety of stress-corrosion tests were performed including smooth-surface, time-to-failure tests; potentiostatic tests on smooth surfaces exposed to constant applied strain rates; and fracture-mechanics-type tests under static and cyclic loads. Both alloys show surface pitting and subsequent intergranular corrosion. Pitting is more severe in the magnesium-bearing alloy and is associated with stringer particles strung along the extrusion direction as a result of P/M processing. Both alloys were found to resist stress-corrosion crack extension at low and moderate stress intensities under conditions of both static and cyclic (high-mean stress) loading. Fatigue-crack growth at low-mean stress is shown to be somewhat environment- and microstructure-sensitive. These results are supported by relevant fractographic and metallographic observations and are discussed in terms of the potentially active stress-corrosion processes.

Introduction

Aluminum-lithium alloys offer the advantages of higher strength and stiffness at low density than existing aerospace alloys. The specific benefits of Al-Li alloys include a potential 20% increase in both the stiffness-to-weight and strength-to-weight ratios. However, little is known about the environmental durability of the Al-Li alloys, particularly when they are exposed to chloride-containing aqueous solutions. Such conditions have caused service problems with the conventional 2000 and 7000 series alloys. Cause for concern in Al-Li alloys is the active lithium-bearing phases which can form. The presence of these active phases at such locations as grain boundaries could result in a significant environmental sensitivity. The present investigation examines these effects and, in particular, the stress-corrosion behavior of Al-Li alloys under a variety of applied electrochemical and mechanical conditions. The purpose of this investigation is not to explore the influence of a single parameter but rather to expose the alloys to a broad range of conditions in order to establish those conditions that may limit the durability of the alloys.

Experimental

Materials and Specimens

Five different Al-Li alloys were investigated having either ingot, powder-metallurgy (P/M), or mechanically alloyed (M/A) product forms. Also investigated was the commercial, ingot aluminum alloy AA7475. The nominal composition and specific product form of each are shown in Table I. Emphasis in the present study was on the two Al-Li-Cu alloys processed using the conventional powder-metallurgy technique. Their compositions are similar except one contains the addition of 1.4% magnesium. Because the stress-corrosion behavior of these two alloys was studied extensively; a number of specimen configurations were required, as will be discussed. The study of the two (M/A) Al-Li alloys, the ingot X-2020 Al-Li alloy and the ingot AA7475 alloy, was limited; they were used primarily to compare the influence of composition and process history and to provide comparison with previously published stress-corrosion data.

The two P/M Al-Li-Cu alloys were received as extruded, rectangular-section, round-cornered bars approximately 12.7 mm thick and 65 mm wide. After solution treatment, the microstructures of both alloys were characterized by columnar-arrays of small, recrystallized grains and stringer particles lying parallel to the longitudinal axis of the bar (extrusion direction), as shown in Figure 1. The mean area density and mean spacing of the stringer particles on a transverse section of the bar are approximately 0.2 μm^{-2} and 7 μm, respectively. It is the spacing of these stringer particles that appears to control both the size and shape of the columnar recrystallized grains (Fig. 1a). The approximate grain diameter is 4 μm and the grain length is approximately 16 μm, for a length-to-diameter ratio of 4:1.

A number of specimen types having various orientations were machined from the P/M Al-Li-Cu alloy bars, as shown in Figure 2. The coordinate system used in this figure to describe orientation is according to ASTM Standard Test Method E399. The orientation of each test specimen is described by a two-coordinate system: the first refers to the direction of the normal to the anticipated crack plane and the second to the direction of crack propagation. As can be seen, specimen configuration and orientation vary widely, as dictated by the specific test objective. The test requirements, including the specific specimen configuration to meet the test objective, will be discussed below.

The two M/A Al-Li alloys (Table I) were received as extruded, square-section, round-cornered rod approximately 19 mm wide. The detailed physical metallurgy of these alloys has been documented elsewhere (1). Briefly, their microstructure is characterized by columnar grains aligned parallel to the extrusion direction. The approximate grain diameter is 0.4 μm and the grain length is about 1.5 μm for a length-to-diameter ratio of 4:1. Aluminum oxide and carbide particles having a total volume content of about 1.5% were randomly distributed throughout the microstructures. Tuning-fork specimens (as depicted in Fig. 2) having an L-S orientation were machined from the bars.

Alloy X-2020 (Table I) was received as a wing-skin obtained from a retired U.S. Navy RA-5C aircraft. The spanwise (wing-tip to wing-tip) direction of the skin was assumed to be the longitudinal direction of the original rolled plate. The microstructure of the alloy was found to consist of very large, pancake-shaped grains, as shown in Figure 3a. The mean grain diameter is about 0.2 mm, with a typical thickness of about 0.03 mm. Tuning-fork specimens (Fig. 2) having the orientation T-S were machined from the plate.

The AA7475 alloy (Table I) was provided by Kaiser Aluminum, Pleasanton, California (Heat 182767) in the form of 8.9-cm-thick forged plate. The microstructure consisted of large-pancake-shaped grains approximately 0.25 mm in diameter and 0.02 mm thick (Fig. 3b). Tuning-fork specimens (Fig. 2) having a T-S orientation were machined from the as-received plate.

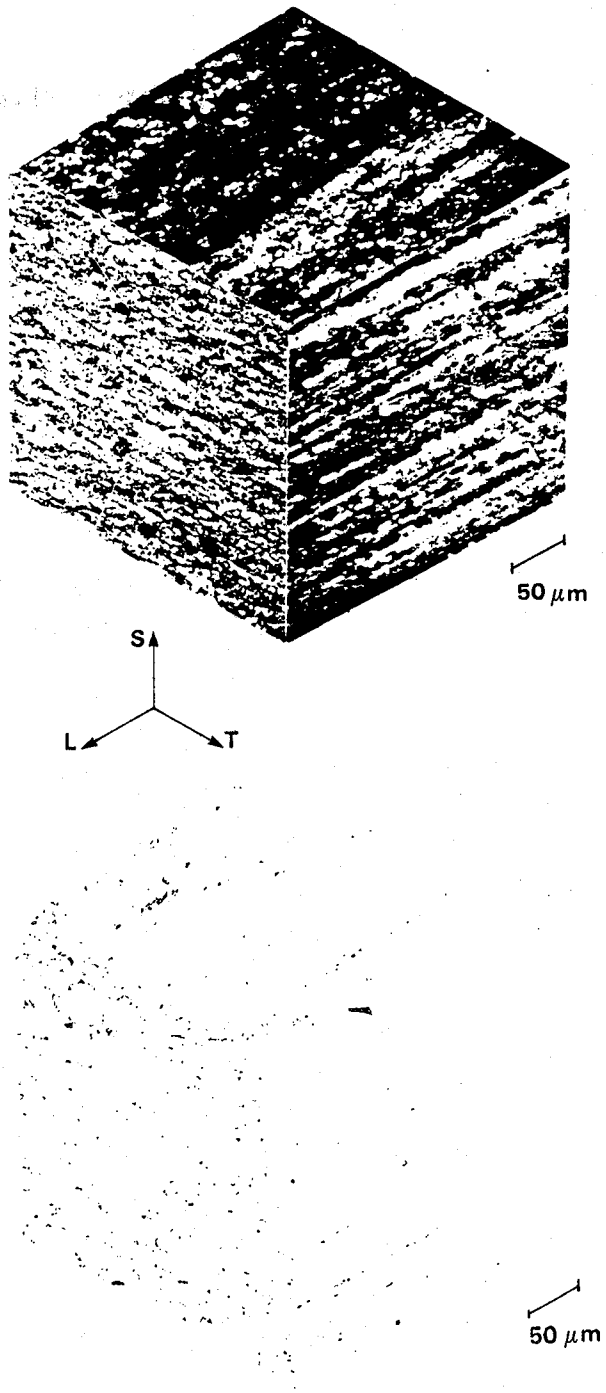

Fig. 1. The columnar grain structure of the P/M processed Al-Li-Cu alloys (a) columnar grains in material etched by Barker's reagent and illuminated by polarized incident light (b) stringer particle array illuminated by nonpolarized light.

Heat Treatment

All alloys were either solution-treated or fully heat treated before specimen fabrication, with the exception of the tuning-fork specimens from the P/M-processed alloys and the X-2020 wing-skin material. In the P/M-processed alloys, residual stresses resulted in excessive distortion, and, thus, a stress relief was required. The stress relief consisted of a 30-min exposure at 450°C, while the material was clamped, followed by an air cool.

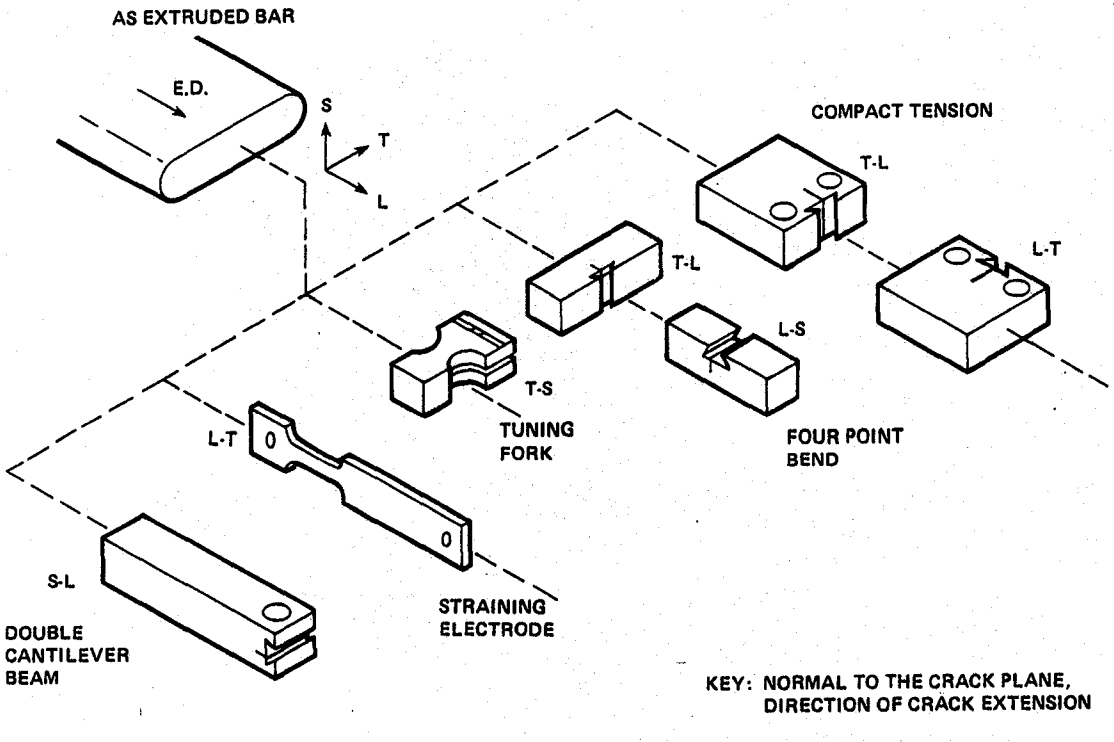

Fig. 2. Orientation of P/M Al-Li-Cu alloy specimens (per ASTM E399).

After fabrication, the tuning-form specimens were solution-treated and quenched in ice water. Approximately 0.38 mm of material was removed from both specimen outer surfaces by polishing with various emery papers. The AA7475 alloy, originally in the -T7351 condition, was heat treated by Kaiser Aluminum to the -T6 condition.

A summary of various heat treatments given the alloys under investigation (Table I) together with their resultant mechanical properties is shown in Table II.

Test Conditions

A variety of test conditions were used, including constant and alternating exposure to the test environment, aerated and deaerated aqueous 3.5% NaCl and synthetic sea water test environments, free corrosion and applied electrochemical potentials, and smooth and flawed specimens of different orientations. The objective was to expose the alloys to a variety of electrochemical and mechanical conditions in order to encourage and identify any environment-enhanced crack initiation and crack-growth process that might occur in service.

Alternate-Immersion Tests. Alternate-immersion tests were performed on tuning-fork specimens primarily to establish the sensitivity of the alloys to crack initiation under free corrosion-potential. Specimens were either loaded to a constant load or a constant deflection and maintained using an appropriate bolt and platen assembly. The load required to establish an initial outer-fiber tensile stress was determined from the respective elastic equation for a cantilever beam. For initial outer-fiber stress levels of 55 Ksi or greater, the constant displacement tuning-fork specimens were usually strain-gauged to provide a more positive method for determining the applied stress. Using the respective value of modulus of elasticity, the outer-fiber stress was determined from measured strain. Specimens displaced to initial outer-fiber stress values less than 55 Ksi were not instrumented.

Table I. Chemical Composition and Product Form of the Aluminum Alloys Studied

Alloy	Product form	Composition, wt %											ppm			
		Nominal alloy composition														
		Li	Cu	Mg	Zr	Si	Fe	Mn	Zn	Ti	Cr	Be	O	Ca	Na	K
Base, P/M Al-Li-Cu	12.7 by 65 mm, round corner, rectangular section bar	2.6	1.4	0.006	0.09	0.03	0.06	0.005	0.02	0.03	0.002	0.005	6	3	2	1
Mg-bearing P/M Al-Li-Cu-Mg		2.6	1.4	1.6	0.09	0.03	0.05	0.005	0.02	0.03	0.002	0.005	5	3	1	1
Mechanically alloyed[a] Al-Li-Mg	19 by 19 mm, round corner, square section rod	2.5	-	1.0	-	-	-	-	-	-	-	-	-	-	-	-
Mechanically alloyed[a] Al-Li-Cu		3.0	2.1	-	-	-	-	-	-	-	-	-	-	-	-	-
X-2020[b] aluminum	Wing-skin from retired RA-5C U.S. Navy aircraft	1.3	4.5	<0.01	-	0.05	0.12	0.70	0.06	0.05	-	-	-	-	-	-
AA7475 Al-Li-Cu-Mg	8.9-cm-thick plate	-	1.4	1.9	-	0.04	0.05	0.001	5.4	0.03	0.24	-	-	-	-	-

[a]Carbon determined by combustion/thermal conductivity is 1.21%; oxygen determined by inert-gas fusion is 0.021 wt %. These concentrations result from the mechanical alloying procedure and can be assumed to be similar in both the copper- and magnesium-bearing alloys.

[b]Additionally, the alloy X-2020 contained 0.21 wt % cadmium.

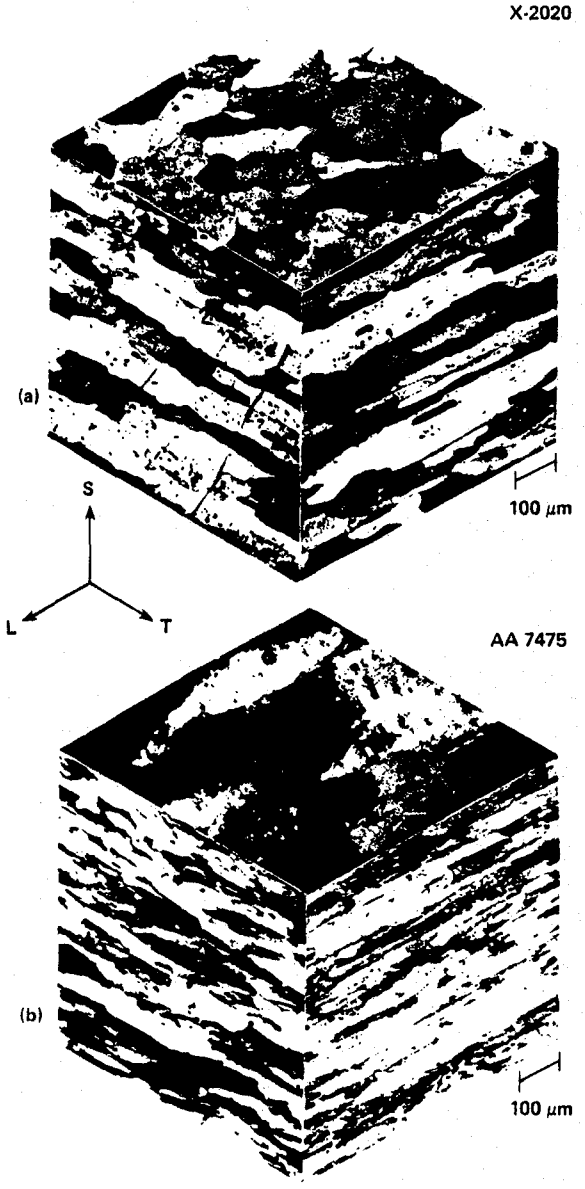

Fig. 3. The grain size and distribution of (a) X-2020 and (b) AA7475 aluminum alloys.

Those specimens were displaced under stroke control in a servohydraulic mechanical test system to a load commensurate with the target outer-fiber stress as determined by the respective elastic equation for a cantilever beam. The resulting tine gap was measured using a feeler gauge accurate to 12 μm. The specimens were then removed and a bolt/platen assembly was used to attain the desired tine closure. Alternate-immersion tests were performed in accordance with ASTM Standard G44 in aerated 3.5% NaCl solution or synthetic sea water (ASTM Specification D1141). In this procedure, specimens are maintained "wet" for 10 min and allowed to dry for 50 min; the cycle is then repeated. Details of the alternate-immersion procedure have been described previously (2).

Constant-Immersion Tests. Crack initiation under constant immersion was studied using both constant-displacement tests and slow-strain-rate tests on smooth specimens. Constant-displacement tests were performed on tuning-fork-type specimens (Fig. 2). Specimens were masked so as to leave an exposed surface area of approximately 0.5 cm^2 on each tensile surface of the specimen and loaded to a constant displacement. The specimen was made the working electrode in a standard polarization cell containing aqueous 3.5% NaCl solution deaerated by helium. After a minimum 1-hr exposure under open-circuit potential, the working electrode was brought to a preselected potential, and the potential was maintained until the specimens failed or the immersion was interrupted. Specimen failure disengaged the potentiostat, thus preserving metallographic and fractographic data. Although the cross-sectional area of the tines of the tuning-fork specimens are reduced during long-term exposure, a concomitant drop in load on the specimen will also occur under constant-displacement conditions. It was determined that these dynamic changes combine to yield an approximately constant outer-fiber stress in the specimen, even after long exposure times.

Slow-strain-rate tests were performed on straining electrode specimens (Fig. 2). These are essentially standard, flat, smooth tensile specimens which were strain gauged and masked so as to leave an exposed surface area of about 0.5 cm^2 on one side of the gauge section. As in the constant-displacement test, the specimen was made the working electrode in a polarization cell. Tests were conducted in deaerated 3.5% NaCl solution, under potentiostatic control, over a range of strain rates from 10^{-4} to 10^{-6} s^{-1}.

Table II. Typical Mechanical Properties of the Al-Li Alloys Studied

Property	P/M processed Al-Li-Cu[a]							Mechanically alloyed Al-Li[b]		Alloy X-2020[c]		AA7475[d]
	Base alloy			Orientation	Mg-bearing							
	Under-aged	Peak-aged	Over-aged		Under-aged	Peak-aged	Over-aged	Al-Li-Cu	Al-Li-Mg	As received	Reheat-treated	Reheat-treated
Yield stress (0.2% offset), MPa	385	460	420		455	520	435	640	600	545	517	430
Ultimate tensile stress, MPa	490	550	490		570	600	550	642	604	580	572	496
Strain to fracture, %	3.5	3.0	5.0		3.5	3.5	4.0	<0.25	0.50	1-3.5	4-6	12.5
Fracture toughness K_Q; MPa-$m^{1/2}$	12	9	8.5	T-L	9.5	8.5	7.5	--	--	21	31	--
	33	--	23	L-T	20.5	17.0	11.5	--	--	--	--	--
	--	18	--	L-S	--	15.5	--	7	10	--	--	--
	11	10	--	S-L	--	--	9	--	--	--	--	34

[a] 1) Tensile data from 6.4-mm-diam standard tensile specimens; fracture toughness from 12.7-mm thick, 25.4-mm compact tension specimens (L-S) oriented. 2) Base alloy specimens solution treated at 515°C for 1 hr then cold-water quenched. 3) Mg-bearing specimens solution treated at 555°C for 1 hr then cold-water quenched. 4) Under-, peak-, and overaged conditions for base alloy: 10, 26, and 200 hr at 170°C, respectively; for Mg-bearing alloy: under-, peak-, and overaged conditions are 5, 26, and 50 hr at 190°C.

[b] 1) Tensile data from 1.7-mm thick flat tensile coupons; fracture toughness from 12.7-mm square section, four-point bend specimens, (L-S) oriented. 2) Al-Li-Cu heat treated at 560°C for 1 hr, cold-water quenched, and aged at 170°C for 2 hr. 3) Al-Li-Mg heat treated at 520°C for 1 hr, cold-water quenched, and aged at 170°C for 2 hr.

[c] 1) Tensile data from 6-mm thick flat tensile coupons; fracture toughness from 12.7-mm thick, 25.4-mm compact tension specimens, (T-L) oriented. 2) Material solution treated at 515°C for 1 hr, cold-water quenched, then aged 18 hr at 170°C.

[d] 1) Tensile data from 6-mm thick flat tensile coupons; fracture toughness from 12.7-mm thick, 25.4-mm compact tension specimens, (S-L) oriented. 2) Heat treatment of the AA7475-T7351 plate to the -T6 condition resulted in an electrical conductivity decrease from 43% IACS to 32% IACS.

Crack propagation under constant-immersion conditons was studied using fatigue precrack, double-cantilever-beam (DCB) specimens; square beam, four-point bend specimens; and compact-tension (CT) specimens (as shown in Fig. 2). The DCB specimens were used to study static crack growth and were maintained under constant-displacement by bolt loading. The details of the test procedure are discussed elsewhere (2). In all cases, the value of the initial applied stress intensity, K_I^i, was at least 1.2 times greater than the maximum stress intensity used during fatigue precracking. Specimens were immersed, loaded, and held in a static 3.5% NaCl solution, exposed to laboratory air, for predetermined times up to 1.4 yr. Final crack length was determined by specimen compliance and fractography.

The square beam, four-point bend specimens were used to study fatigue crack growth at high values of mean-stress intensity. The specimens were initially fatigue precracked in air to a ratio of crack length to specimen width (a/w) of about 0.35. Before fatigue precracking, the specimen side surfaces were polished to 1 μm diamond and the specimen was masked such that the crack mouth and a rectangular strip along the anticipated crack path on one side of the specimen were exposed. This allowed for potentiostatic control along the region of the crack mouth. The specimen was immersed in helium deaerated 3.5% NaCl solution and loaded to a minimum stress intensity, K_I^m, equal to 90% of the maximum cyclic stress intensity, K_I^M, to be applied. The initial value of K_I^M was always at least 1.2 times greater than the maximum stress intensity used during fatigue precracking. After about 2 hr of constant immersion at the free corrosion-potential, the specimen was driven more noble, inducing anodic dissolution. These potentials ranged from -0.790 to -0.850 V (sce) and induced an anodic current of about 2 to 50 μA. Specimens were ramp-loaded under load control to the predetermined K_I^M, over a 10-min period, at which time the load was rapidly dropped (within 3 sec) to K_I^m, and the cycle repeated. Crack-opening displacement was monitored using a clip-gauge, and compliance data were used to assess crack extension. After a minimum of 20 cycles, specimen compliance was reassessed to determine whether crack extension had occurred. At increments of no less than 3 hr, the stress intensity values were increased, with K_I^m remaining at 90% of K_I^M. In this manner, an attempt was made to induce environment-enhanced fatigue-crack growth at high mean-stress intensities.

Compact tension (CT) specimens (Fig. 2) were used to assess environment-enhanced fatigue-crack growth at low mean-stress intensities. Specimens were fatigue-tested at a minimum-to-maximum-load ratio, R, of 0.1, using a sinusoidal waveform, in either laboratory air or in an aqueous 3.5% NaCl solution, using an intermittent drip technique. That is, the salt solution was introduced into the fatigue crack through a cotton-cloth syphon placed adjacent to one face of the compact-tension specimen. The cotton was kept moist by capillary feed from a 500-ml reservoir of NaCl solution and by intermediate drip feed from a second 500-ml reservoir through an appropriate needle valve and Luggin capillary tube. Tests were performed under load control using a servohydraulic mechanical test system employing computer feedback and control. Using both compliance and load data for the compact-tension configuration, the computer was programmed to maintain a constant value of alternating stress intensity factor ΔK over a preprogrammed range of crack extension. The minimum range of crack extension for determination of steady-state crack growth rate behavior was 0.75 mm. The usable data acquisition range was from 0.32 to 0.60 of the crack-length to specimen-width ratio (a/w). Data were acquired at each 50 μm of crack extension.

Metallography

Metallography was performed to evaluate the character of stress-corrosion cracking in the various alloys. Standard metallographic techniques

were used. Keller's etch, diluted to different concentrations according to the nature of the reactivity of each alloy, was used for standard immersion etching. The mechanically alloyed Al-Li alloys were most active in that they were etched during final polishing (0.3 μm alumina) by exposure to water. A 6:1 dilution of standard Keller's etch provided optimum etching of the M/A Al-Li; 3:1 for P/M Al-Li-Cu, 4:1 for X-2020 aluminum and full-strength for the AA7475 -T6 aluminum. It is of interest to note that in the case of the P/M Al-Li-Cu alloy, selective etching of shear-deformation bands was observed. The effect was not immediate, but occurred from 5 to 12 hr after etching with Keller's reagent; the effect was reproducible. This phenomenon is further discussed in the Results section.

Some specimens were electropolished in Barker's reagent, and polarized light illumination was employed to examine the grain structure of the various alloys. Electropolishing was performed at 40 Vdc in a solution of 5 ml of 48% HBF_4 and 200 ml of distilled water; a current density of about 200 mA/cm^2 resulted.

Results

Alternate-Immersion Tests

Alternate-immersion tests were performed under free corrosion-potential in aerated NaCl solutions on all six of the study alloys. The results of these tests are presented in Figure 4 for the P/M Al-Li-Cu alloy in 3.5% NaCl solution and synthetic sea water; in Figure 5 for the P/M Al-Li-Cu-Mg alloy in the same two solutions; in Figure 6 for the two M/A alloys in synthetic sea water; in Figure 7 for the X-2020 alloy in synthetic sea water; and in Figure 8 for the AA7475 alloy in synthetic sea water. These figures show the condition of the specimens (failed, cracked, or unaffected) after various times at different stress levels. For comparison, the free corrosion-potentials (with respect to the standard calomel electrode) are given in

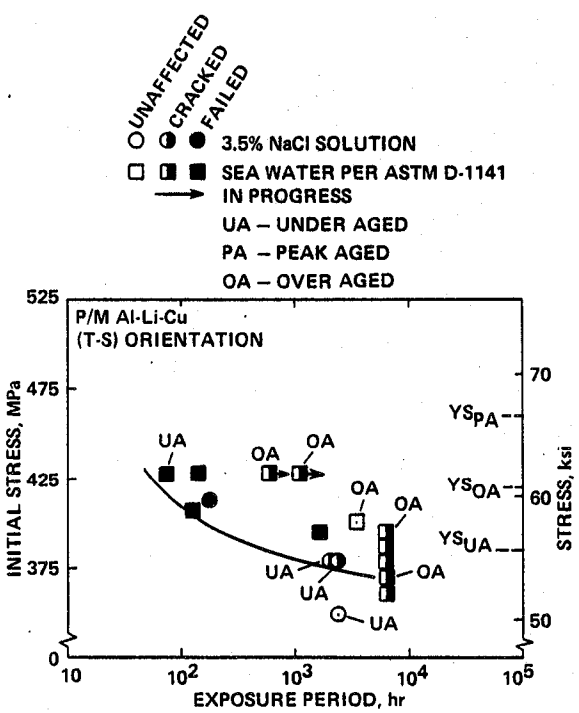

Fig. 4. Alternate-immersion data for the P/M Al-Li-Cu alloy.

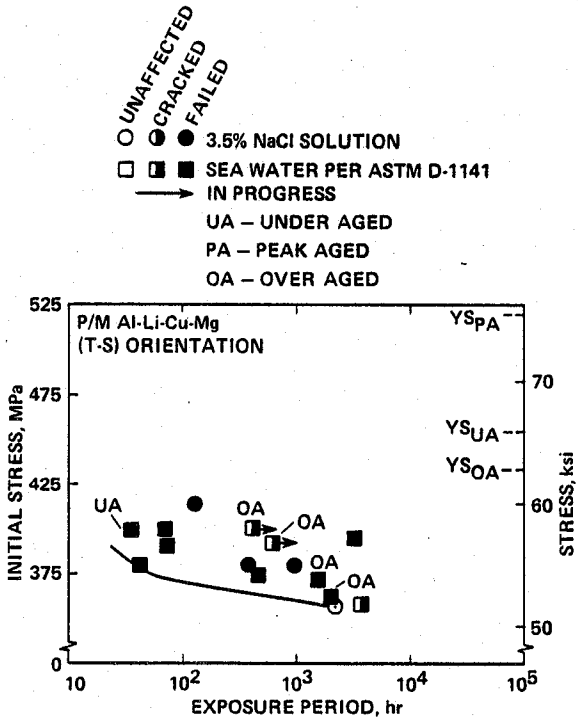

Fig. 5. Alternate-immersion data for the magnesium-bearing P/M alloy.

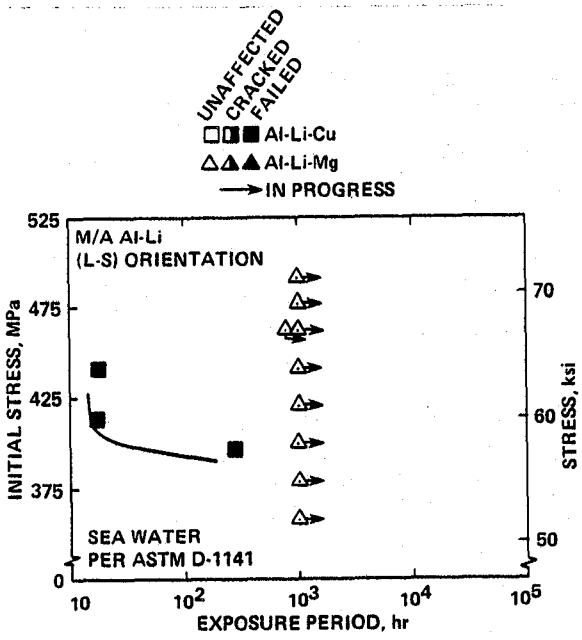

Fig. 6. Alternate-immersion data for the mechanically alloyed Al-Li alloys.

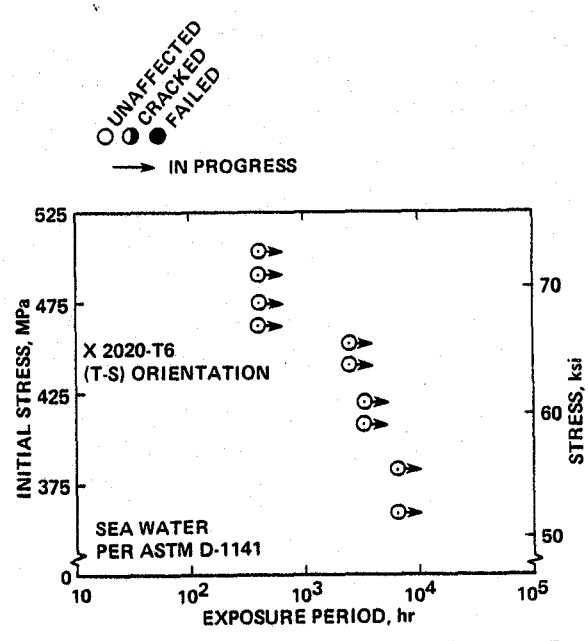

Fig. 7. Alternate-immersion data for X2020-T6 alloy.

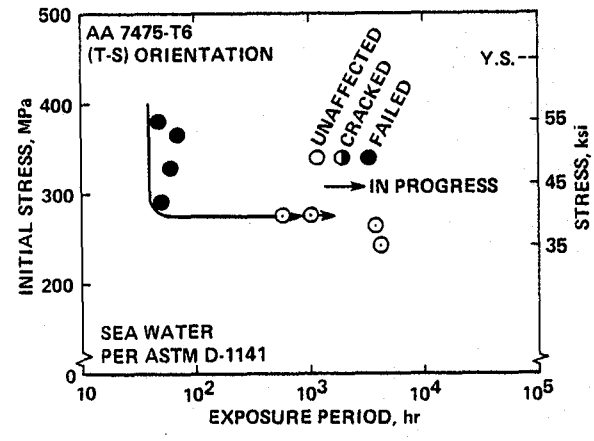

Fig. 8. Alternate-immersion data for the AA7475-T6 aluminum alloy.

Table III. Finally, Figure 9 is a summary of the lower-limit failure curves obtained from the above figures for all six alloys. Comparison of the lower-limit curves of Figure 9 demonstrates that alloy X-2020 and the M/A Al-Li-Mg alloy are very resistant to stress-corrosion cracking. The P/M base and Mg-bearing alloys, AA7475 and the M/A Al-Li-Cu alloy are susceptible, the AA7475 being the most susceptible.

The effect of aging on the stress-corrosion behavior of the two P/M Al-Li-Cu alloys was explored in the alternate-immersion tests. Comparison of the underaged, peak-aged, and overaged conditions for the P/M Al-Li-Cu and P/M Al-Li-Cu-Mg is provided in Figures 4 (Al-Li-Cu) and 5 (Al-Li-Cu-Mg). The stress-corrosion resistance is found to increase with aging time for the three conditions investigated, the underaged material having the shortest lifetime. The overaged specimens either took longer to fail or remained unfailed after prolonged exposure. This difference in stress-corrosion resistance as a function of aging time appears to be greater at higher applied stress (Figs. 4 and 5).

Multicrack initiation on the tensile surface of failed tuning-fork specimens typical of both P/M Al-Li-Cu alloys is illustrated in Figure 10. Stress corrosion cracks representative of those found are depicted in Figure 11. Intergranular cracking was neither found on the compression-side of tuning-fork tines nor on exposed, nonstressed surfaces. Metallographic examination showed no secondary cracking of the failed M/A Al-Li-Cu specimens. The surfaces of the M/A Al-Li-Mg alloy specimens were only mildly pitted for exposures up to 1000 hr. Similarly, the exposed surfaces of the X2020-T6 specimens were uncracked and only mildly pitted.

Table III. Representative Free Corrosion-Potentials of Tuning-Fork Specimens in the Alternate-Immersion Tests

Alloy	Heat treatment	V_o, V[a]
P/M Al-Li-Cu	Underaged	-0.800
	Peak-aged	-0.738
	Overaged	-0.763
P/M Al-Li-Cu-Mg	Underaged	-0.765
	Peak-aged	-0.750
	Overaged	-0.808
M/A Al-Li-Cu	2 hr at 170°C	-0.785
M/A Al-Li-Mg	2 hr at 170°C	-0.854
AA7475	-T6	-0.746
X-2020	-T6	-0.763

[a]All potentials measured with respect to the standard calomel electrode in flowing sea water solution (per ASTM Specification D1141); standard deviation is typically 0.035 Vdc for a given alloy/heat-treatment condition.

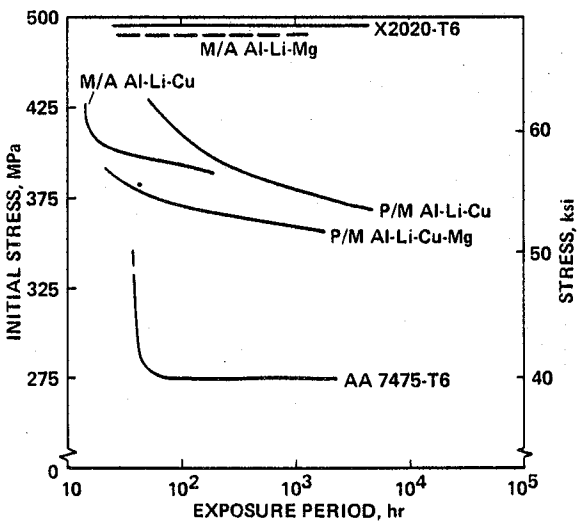

Fig. 9. A comparison of the stress-corrosion susceptibility of the alloys investigated.

Fig. 10. Multicrack initiation on the tensile surface of an Al-Li-Cu alloy tuning fork specimen after 84-day alternate-immersion exposure in aqueous 3.5% NaCl solution.

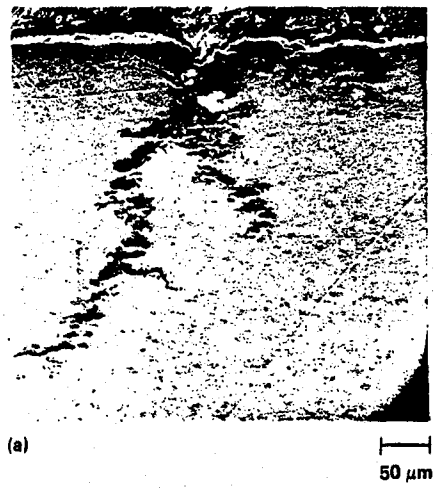

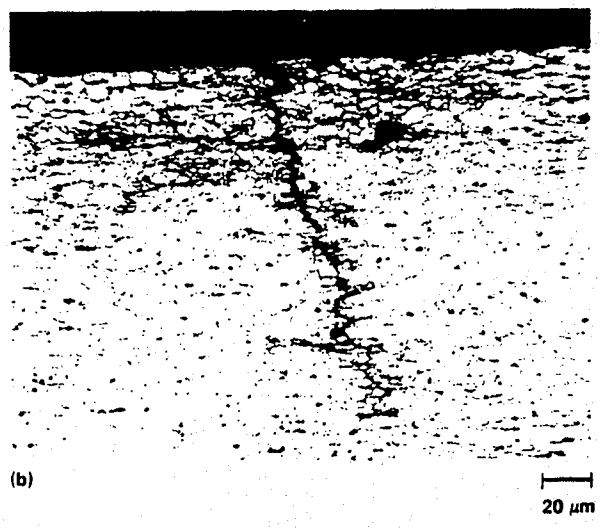

Fig. 11. Stress corrosion cracks in the Al-Li-Cu-Mg alloy; transverse section of tuning fork tine (a) SEM micrograph of a surface crack (b) optical micrograph of a second crack indicating the intergranular, multibranched fracture path.

The size of the deepest intergranular cracks occurring in the P/M Al-Li-Cu alloys (Fig. 11) was typically 0.38 mm; this depth is comparable to the critical flaw size estimated from the known fracture toughness of these alloys (Table II). Since low fracture toughness precludes the growth of sharp cracks beyond approximately 0.3 mm, the life of the P/M Al-Li-Cu tuning-fork specimens is essentially limited by crack-initiation events.

Constant-Immersion Tests

Crack Initiation. Crack initiation under selected electrochemical conditions was investigated using the tuning-fork specimens of the P/M alloys. Tests were conducted under constant displacement and with potentiostatic control in a deaerated 3.5% NaCl solution. Two tests on the P/M Al-Li-Cu alloy are in progress, both at an electrochemical potential of -0.790 V (sce) and at an initial outer-fiber stress of 424 MPa. After 2000 hr (well beyond failure in alternate-immersion tests (Fig. 4)) neither specimen has failed. Inspection has revealed some localized corrosion along stringer particles, but gross pitting has not been detected. This electrochemical potential is in the anodic passivation regime.

Similar tests were performed on the magnesium-bearing P/M alloy. Two tuning-fork specimens were initially stressed to 403 MPa, and one was exposed to an anodic potential of -0.800 V (sce) and the other to a cathodic potential of -1.015 V (sce). The average specimen current density for each test was approximately the same — about 50 $\mu A/cm^2$. Both specimens failed within 1200 hr. This failure time is substantially longer than that observed at a similar stress level under alternate-immersion test conditions (Fig. 5). Metallographic examination of the specimen that failed under anodic polarization revealed secondary branch-cracking similar to that observed in the alternate-immersion tests (Fig. 11). A cell-current and temperature excursion accompanying failure of the P/M Al-Li-Cu-Mg specimen tested under cathodic polarization obscured efforts to document the failure mode.

Slow-strain-rate tests were performed in an attempt to identify polarization conditions that may induce crack initiation in the P/M Al-Li-Cu alloy. The results of these tests, shown in Figure 12, have been reported elsewhere (2). As can be seen, a ductility loss is only observed at an anodic potential at which passive film-formation occurs in the deaerated 3.5% NaCl solution. A current density of no more than 5 $\mu A/cm^2$ is involved in this

passivation process and localized pitting occurs at the stringer particles. Eventually, large randomly spaced pits develop from stringer particle pits, and subsequent fracture occurs. Intergranular cracking is associated with the randomly spaced pits, but the extent of intergranular cracking is much less than the critical flaw size based on fracture toughness data (2). Slow-strain-rate tests performed at the free corrosion-potential or within the cathodic regime at current densities equivalent to those within the anodic-passive region resulted in fracture strains equivalent to those observed in laboratory air control tests.

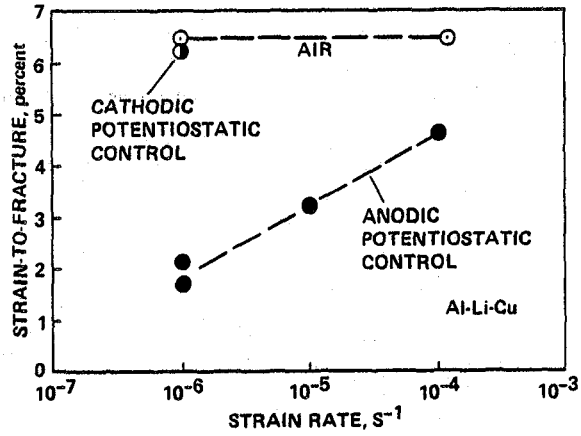

Fig. 12. The apparent stress corrosion susceptibility of P/M Al-Li-Cu at various applied potentials; slow strain-rate data.

Crack Propagation. Crack propagation under constant-immersion conditions was studied using a variety of precrack specimens. The particular specimen configuration was dictated primarily by the desired crack plane and growth orientation. For example, the L-S-oriented, four-point-bend specimens (Fig. 2) were used to permit the crack plane to be perpendicular to the stringer particle arrays in the P/M alloys. Use of DCB specimens (Fig. 2) allowed investigation of slow crack extension in the S-L orientation, whereas the CT specimens (Fig. 2) were used for the T-L and L-T orientations. Additionally, the DCB specimens are readily bolt-loaded to a fixed displacement and are ideal for long-term exposures.

An attempt was made to investigate static crack growth and to establish the threshold stress intensity for stress-corrosion cracking, K_{ISCC}, in the P/M alloys using DCB, S-L-oriented specimens. Tests were conducted in an aerated 3.5% NaCl solution under free corrosion-potential. The results of these tests are summarized in Table IV. As can be seen, crack growth was observed. A study of the deformation mode and fracture characteristics of these specimens suggests, however, that the process is more one of localized corrosion and mechanical tearing (2). Because the fracture toughnesses of these alloys in the S-L orientation are very low (Table II), the values of K_I^f cannot be taken to be a valid indication of K_{ISCC}.

Table IV. Time-Dependent Crack Growth of DCB Specimens in Aqueous 3.5% NaCl Solution

Alloy	Aged condition	35-day immersion			159-day immersion		
		K_I^i, MPa-$m^{1/2}$	K_I^f, MPa-$m^{1/2}$	Δa, mm	K_I^i, MPa-$m^{1/2}$	K_I^f, MPa-$m^{1/2}$	Δa, mm
Al-Li-Cu	Under	9.0	7.5	3.0	9.5	7.5	2.5
Al-Li-Cu	Peak	11.0	9.0	0[a]	9.0	8.5	0.8
Al-Li-Cu-Mg	Over	7.0	5.5	4.0	10.5	7.5	4.0

Note: K_I^i: crack-tip stress-intensity factor applied prior to immersion period; K_I^f: crack-tip stress-intensity factor at termination of the immersion period.

[a]Exhibited pop-in during loading.

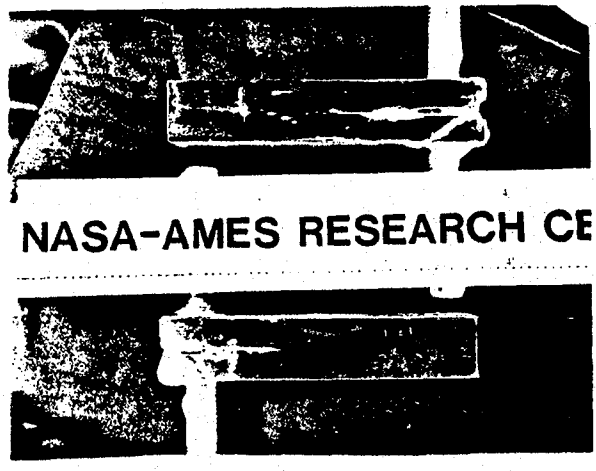

Fig. 13. Constant-immersion DCB specimens exposed 1.4 yr in 3.5% NaCl solution; base (lower) and magnesium-bearing (upper) alloy specimens. Approximately 0.5 mm removed by grinding, then polished to 1 μm alumina.

The physical appearance of the S-L-oriented DCB specimens that underwent long-term exposure (1.4 yr) to the aqueous NaCl environment is shown in Figures 13-17. The magnesium-bearing alloy was found to be very susceptible to localized pitting, much more so than the base alloy, as shown in Figure 13. Metallographic examination of the rough-polished side-surfaces of the DCB specimens, perpendicular to the pre-crack plane, indicate extensive intergranular cracking and corrosion, both in the P/M Al-Li-Cu alloy, as shown in Figures 14 and 15, and in the magnesium-bearing alloy, as shown in Figures 16 and 17. The intergranular attack is again associated with the stringer particles aligned parallel to the extrusion direction. Intergranular attack is not localized to the region of crack growth but occurs at selected regions along the crack plane, as shown in Figure 17. In the P/M Al-Li-Cu alloy, intergranular corrosion is more intense in the slip deformation bands developed during fatigue precracking process, as shown in Figure 14.

Fatigue-crack growth in the P/M Al-Li-Cu alloys was studied at high values of mean-stress intensity and at very low frequencies, using fatigue precracked, four-point bend specimens. One specimen, L-S oriented, from each alloy was tested under potentiostatic control in a deaerated NaCl solution. The specific test conditions and the number of applied cycles at each condition are shown in Table V. On the basis of specimen compliance, no

Table V. Test History of the P/M Aluminum-Lithium Four-Point Bend Specimens Fatigued at High K_I^M and High mean Stress R

	V_{sce}, Vdc	i_{anodic}, μA	K_I^M, MPa-$m^{1/2}$	R	ΔN, cycles
P/M Al-Li-Cu	-0.792	8	10.3	0.93	130
Base alloy	-0.792	25	11.5	0.94	20
(K_{IQ} = 18 MPa-$m^{1/2}$)	-0.792	32	12.4	0.95	10
	-0.851	7	14.3	0.95	70
	-0.851	26	15.4	0.96	20
				-Termination-	
P/M Al-Li-Cu-Mg	-0.790	12	6.6	0.90	127
Mg-bearing alloy	-0.790	42	7.7	0.91	25
(K_{IQ} = 15.5 MPa-$m^{1/2}$)	-0.790	45	8.8	0.91	25
	-0.790	64	9.3	0.92	35
	-0.800	145	9.9	0.92	80
	-0.840	50	10.4	0.93	20
	-0.840	70	12.3	0.94	10
	-0.855	70	13.4	0.95	25
	-0.840	75	13.7	0.95	80
	-0.840	75	15.0	0.95	30
	-0.840	75	15.4	0.95	20
				-Termination-	

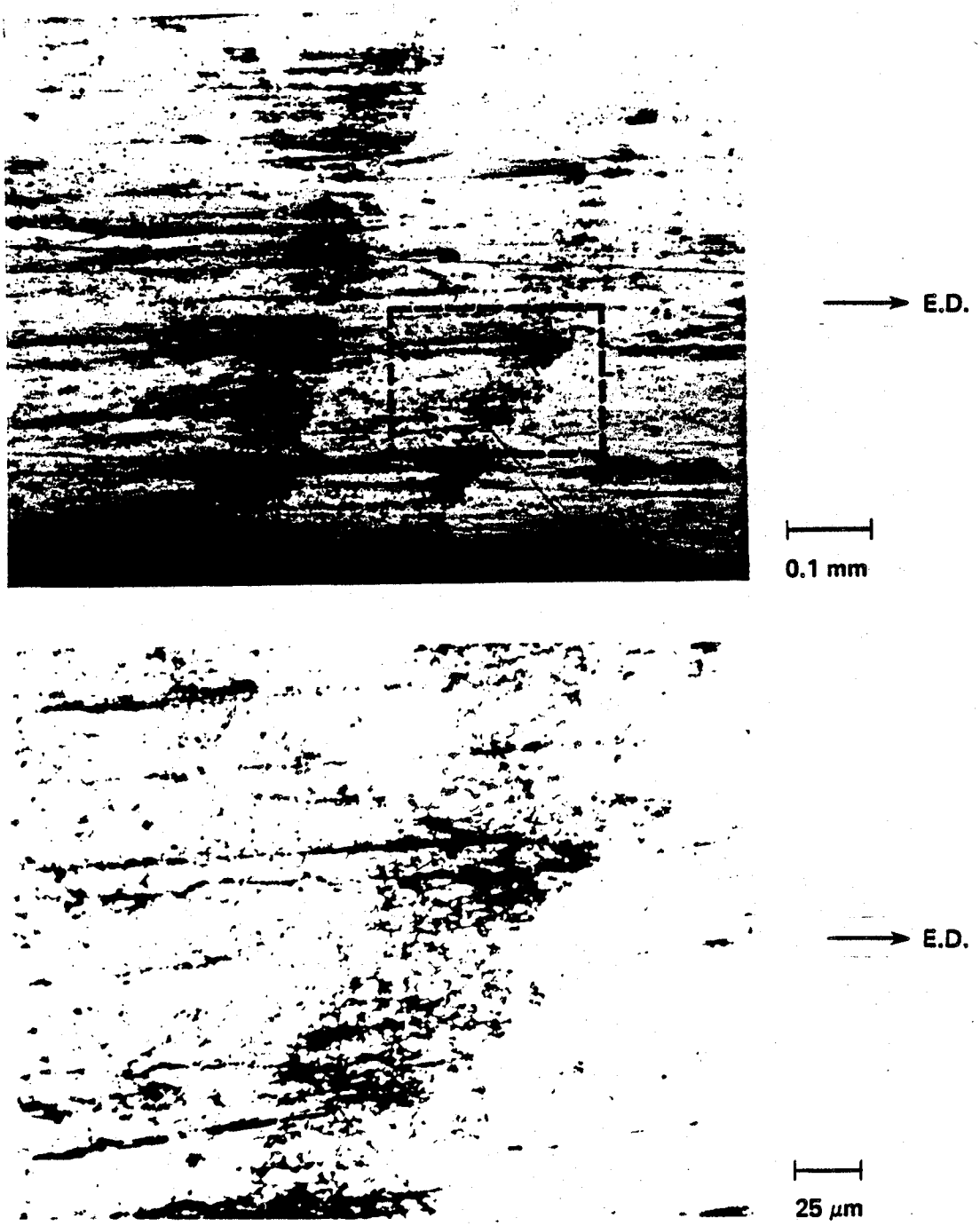

Fig. 14. Intergranular corrosion along shear-deformation bands in Al-Li-Cu base alloy DCB specimen immersed 1.4 years in 3.5% NaCl solution (as polished); (a) corroded slip deformation bands adjacent precrack crevice and (b) close-up of intergranular corrosion within band.

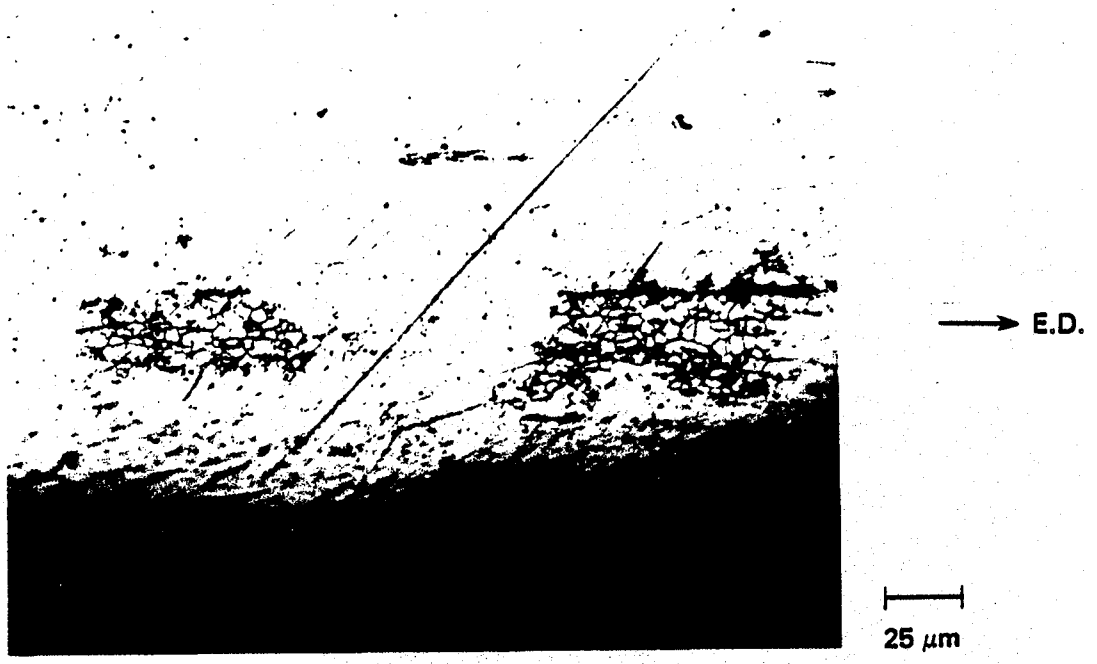

(a)

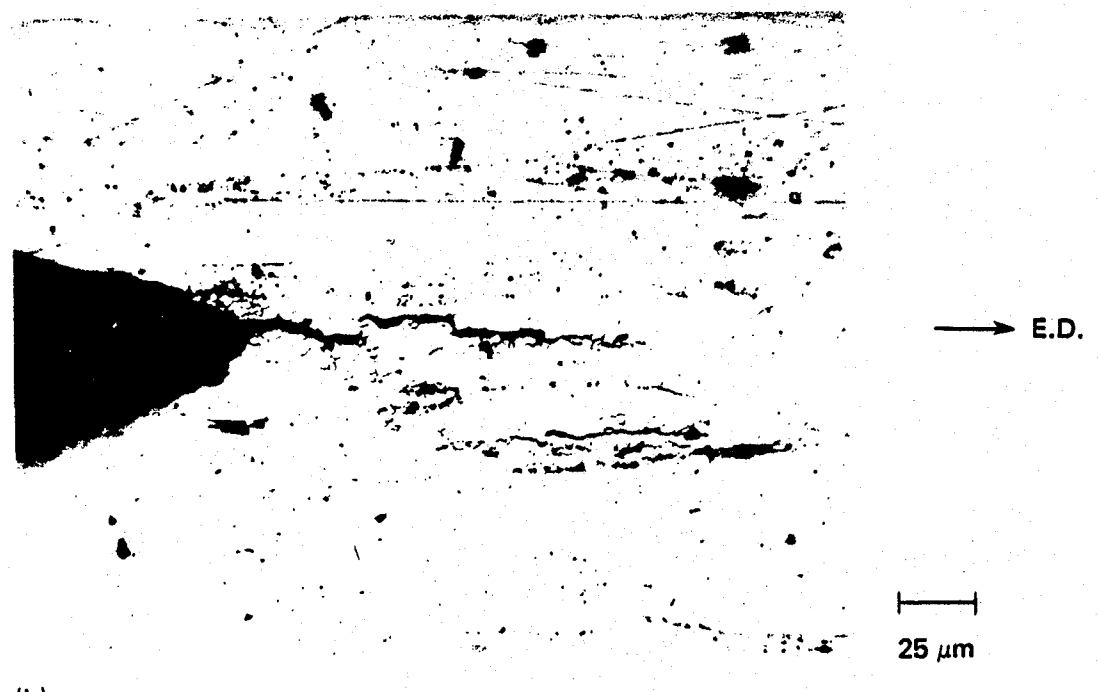

(b)

Fig. 15. Intergranular corrosion (a) adjacent machined notch and (b) at crack-tip of P/M Al-Li-Cu alloy DCB specimen (as polished).

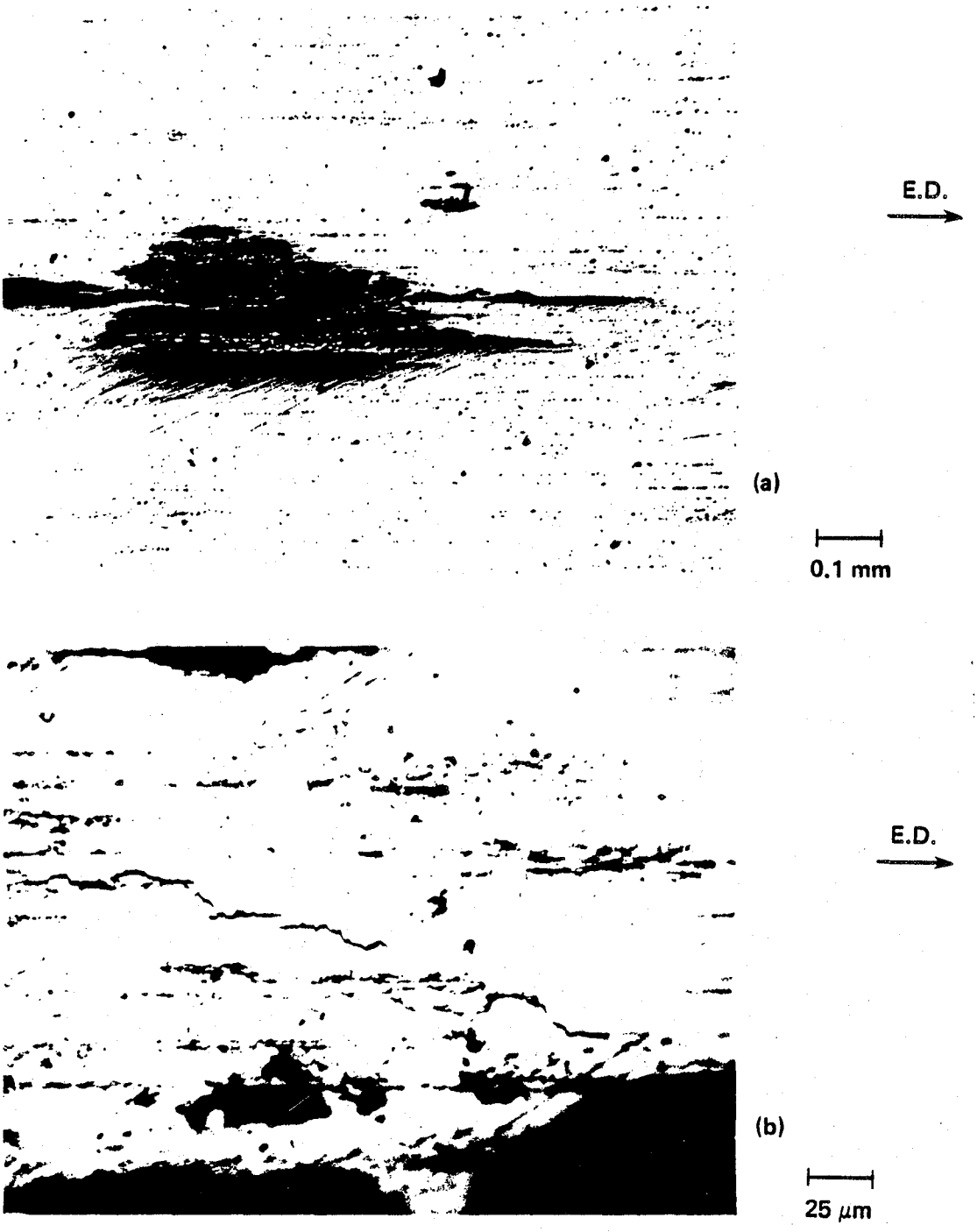

Fig. 16. Localized corrosion and intergranular cracking at crack tip of P/M Al-Li-Cu-Mg DCB specimen (as polished); (a) crack tip and (b) intergranular cracking in near crack-tip region.

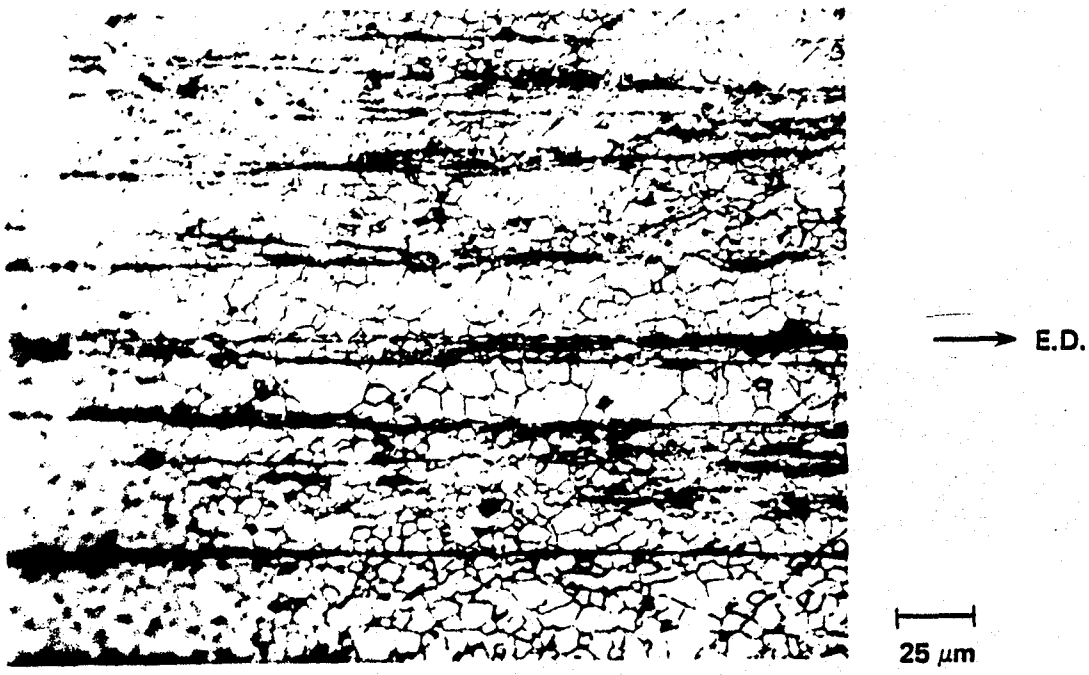

Fig. 17. Intergranular corrosion along stringer oxide particles adjacent fatigue precrack crevice in P/M Al-Li-Cu-Mg DCB specimen (as polished).

measurable crack extension occurred in either the base or magnesium-bearing alloy.

After testing, metallographic studies were performed on both specimens; the significant observations are reported in Figures 18 and 19. These figures represent sections taken at the polished and etched mid-thickness plane of the four-point bend specimens. Intergranular cracking did occur in both alloys, but along the stringer particles, perpendicular to the main crack-plane. Cracking was not localized near the tip of the fatigue precrack, but was present rather uniformly along the precrack crevice. Intergranular cracking was prevalent at the mid-thickness plane of the specimens, and the magnesium-bearing alloy exhibited the more pronounced cracking.

Fatigue-crack growth at low mean-stress intensities was studied in the two P/M Al-Li-Cu alloys using L-T and T-L compact-tension specimens (Fig. 2). The objective of these tests was to determine whether 3.5% NaCl solution would affect the steady-state crack-growth rate behavior at a given value of stress-intensity range ΔK. Laboratory air was taken to be the "dry" control condition. All tests were performed at 1 Hz. The base alloy specimens were in the overaged (200 hr at 170°C) heat-treatment condition; the magnesium-bearing alloy specimens were peak-aged 24 hr at 190°C. The respective fatigue-crack growth data for the base and magnesium-bearing alloys are presented in Figures 20 and 21, respectively; data for the two alloys are compared in Figure 22.

The curves of Figure 20 demonstrate that the fatigue-crack-growth rate behavior of the P/M Al-Li-Cu alloy is dependent on both specimen orientation and environment. For a given value of stress-intensity range, crack growth occurs more rapidly in the T-L oriented specimens. Similarly, for a given value of stress-intensity range, specimens exposed to aqueous sodium chloride solution grow at a faster rate than those exposed to laboratory air. The degree of environmental influence is not uniform over the range of ΔK investigated. This is due to a change in shape of the crack-growth rate versus ΔK trend curves for both wet and dry conditions and for both

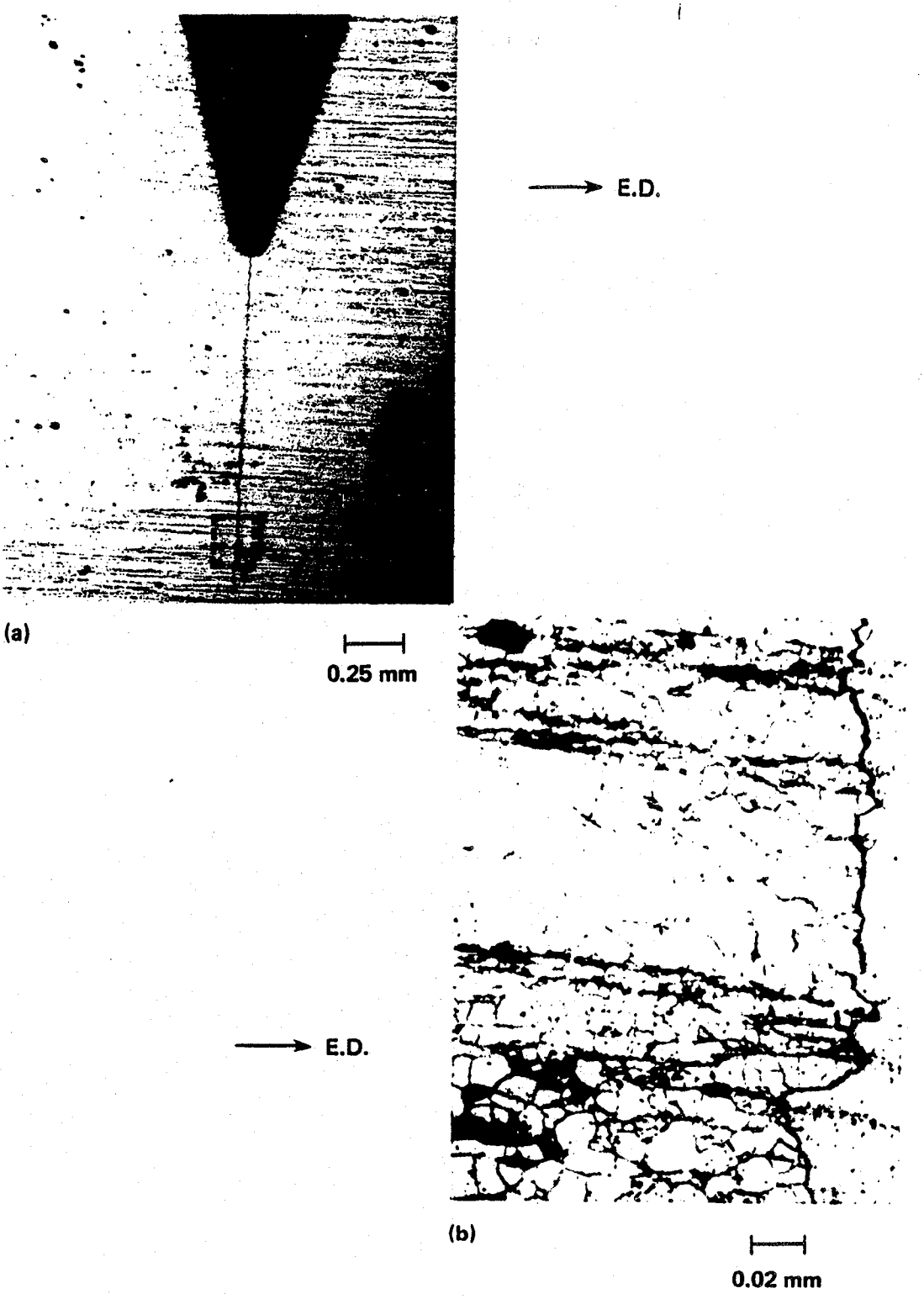

Fig. 18. Intergranular corrosion in fatigues P/M Al-Li-Cu four-point bend specimen (R~.95) at mid-thickness after 2 day exposure in He-deaerated 3.5% NaCl solution under potentiostatic control (a) machined notch and fatigue pre-crack (b) intergranular corrosion adjacent fatigue pre-crack.

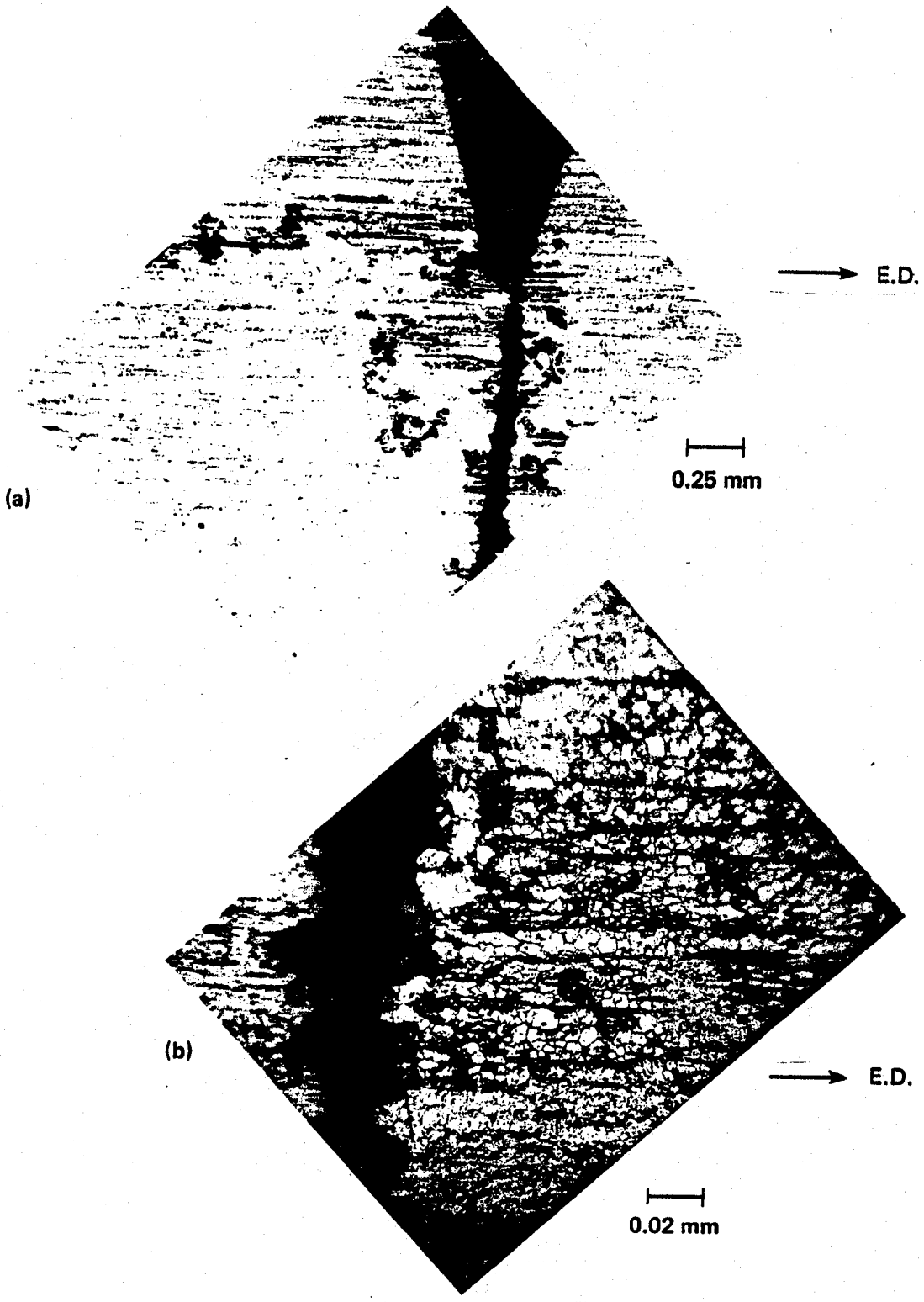

Fig. 19. Intergranular corrosion in fatigued P/M Al-Li-Cu-Mg four-point bend specimen (R~.95) at mid-thickness after 3 day exposure in He-deaerated 3.5% NaCl solution and under potentiostatic control (a) machined notch and fatigue pre-crack (b) intergranular corrosion adjacent fatigue pre-crack.

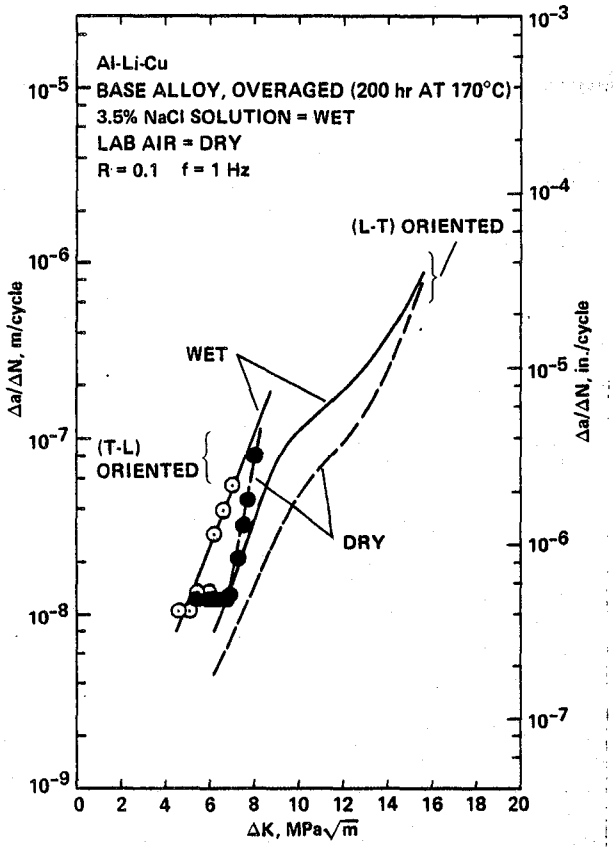

Fig. 20. Fatigue crack growth behavior of the P/M Al-Li-Cu alloy for both wet and dry test conditions.

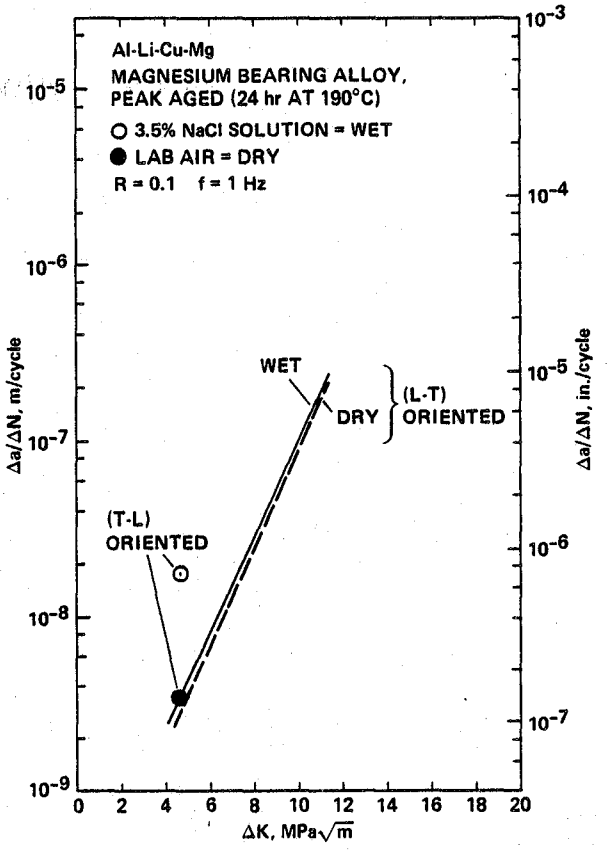

Fig. 21. Fatigue crack growth behavior of the P/M Al-Li-Cu-Mg alloy for both wet and dry test conditions.

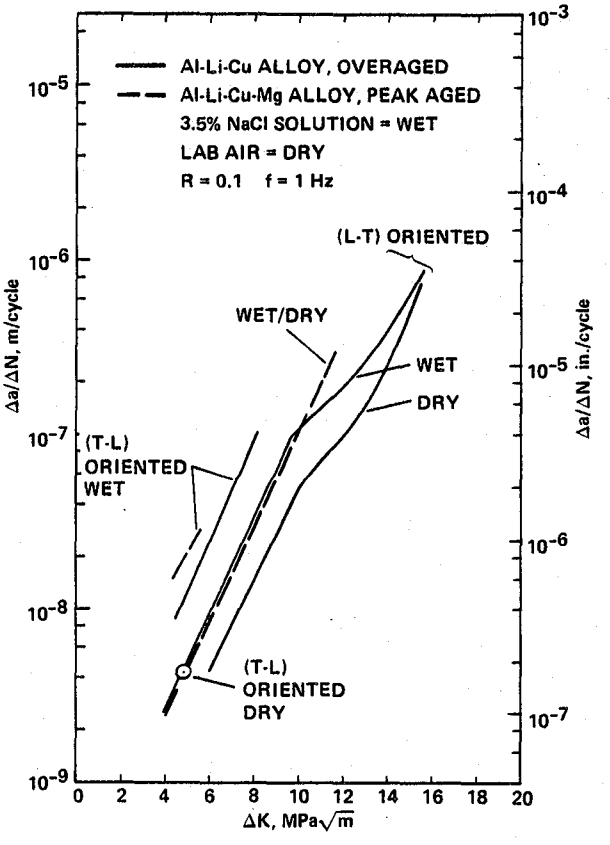

Fig. 22. A comparison of fatigue crack growth behavior for the P/M processed Al-Li-Cu alloys.

specimen orientations. The maximum environmental influence occurs at some intermediate ΔK value and is equal to an increase in fatigue crack growth rate by a factor of about 2.

The fatigue-crack growth behavior of the magnesium-bearing alloy is presented in Figure 21. Unlike the base alloy, the crack-growth rate appears to be relatively unaffected by specimen orientation. Additionally, the L-T-oriented specimens, whether wet or dry, test the same. A definite environment-induced increase in crack-growth rate occurs only in the T-L-oriented specimens. The data suggest a potential fivefold increase in crack-growth rate for a given value of stress-intensity range when aqueous sodium chloride is introduced into a growing crack.

Fatigue-crack-growth rate behaviors of the two P/M Al-Li-Cu alloys are directly compared in Figure 22. Two features which distinguish the fatigue-crack growth behavior of the base alloy are 1) the change in shape of the trend curves for both wet and dry conditions at high values of ΔK, and 2) the relatively higher fatigue-crack growth resistance in laboratory air. The trend curves for the base alloy break from linearity at approximately the same value of stress-intensity range (10 MPa-$m^{1/2}$). Metallographic data will next be presented to show that a change in fracture morphology accompanies this change in fatigue-crack growth behavior for the base alloy.

After testing, the CT specimens were loaded to fracture and scanning-electron-microscope (SEM) fractography was performed. A typical fracture surface of an L-T oriented P/M Al-Li-Cu alloy specimen is shown in Figure 23. It is in this alloy and this orientation that a shift in the fatigue-crack-growth rate curves (wet and dry) occur at ΔK values greater than about 10 MPa-$m^{1/2}$ (Fig. 22). As can be seen in Figure 23, at high values of ΔK the crack proceeds along two planes: the main crack plane, whose normal is the L-direction, and the secondary crack planes whose normals are approximately the S-direction. At low values of ΔK (<10 MPa-$m^{1/2}$) fracture proceeds solely along the main crack plane. The brittle nature of the secondary cracks in the high ΔK regions (ΔK^1 retions of Fig. 23) and their association with stringer particles can be seen in Figure 24.

In addition to the macroscopic secondary cracking at ΔK values greater than about 10 MPa-$m^{1/2}$, the P/M Al-Li-Cu alloy exhibits a high density of microscopic secondary cracks. Such cracking, in a region removed from the macroscopic fracture ridges, is depicted in Figure 25. In order to investigate the nature of these microscopic cracks, metallographic sections transverse to the main crack plane were prepared. A typical section within a crack-growth region where ΔK exceeded 10 MPa-$m^{1/2}$ is shown in Figure 26. Two characteristic features were observed: 1) microcracks present along the stringer oxide particles, and 2) intense shear-deformation bands intercepting the main-crack plane at approximately 45°. Microcracks such as those seen in Figure 26 correlate with the microscopic secondary cracks shown in Figure 25. Unlike the microscopic secondary cracks, the intense shear-deformation bands appeared in the base alloy regardless of the magnitude of the applied stress-intensity range.

Metallographic examination was performed on the P/M Al-Li-Cu-Mg alloy compact-tension specimens of the fatigue-crack-growth study. Macroscopic secondary cracking similar to that observed for the base alloy (Fig. 24) was not found in the magnesium-bearing alloy. However, it is noted that testing at ΔK values greater than about 10 MPa-$m^{1/2}$ was limited in the magnesium-bearing alloy because of 1) the lower fatigue-crack-growth resistance of the alloy (Fig. 22) and 2) the reduced fracture toughness (Table II) with respect to the base alloy. At the higher ΔK values, microscopic secondary cracking,

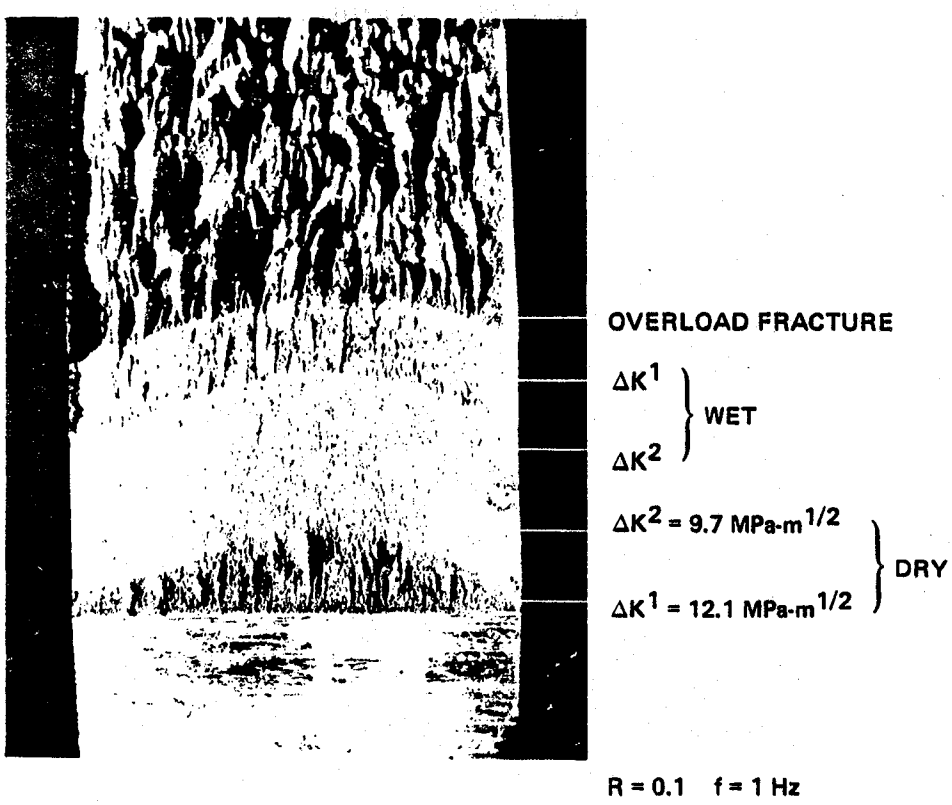

Fig. 23. Transition in FCG fracture morphology of a P/M Al-Li-Cu alloy, L-T oriented, CT specimen.

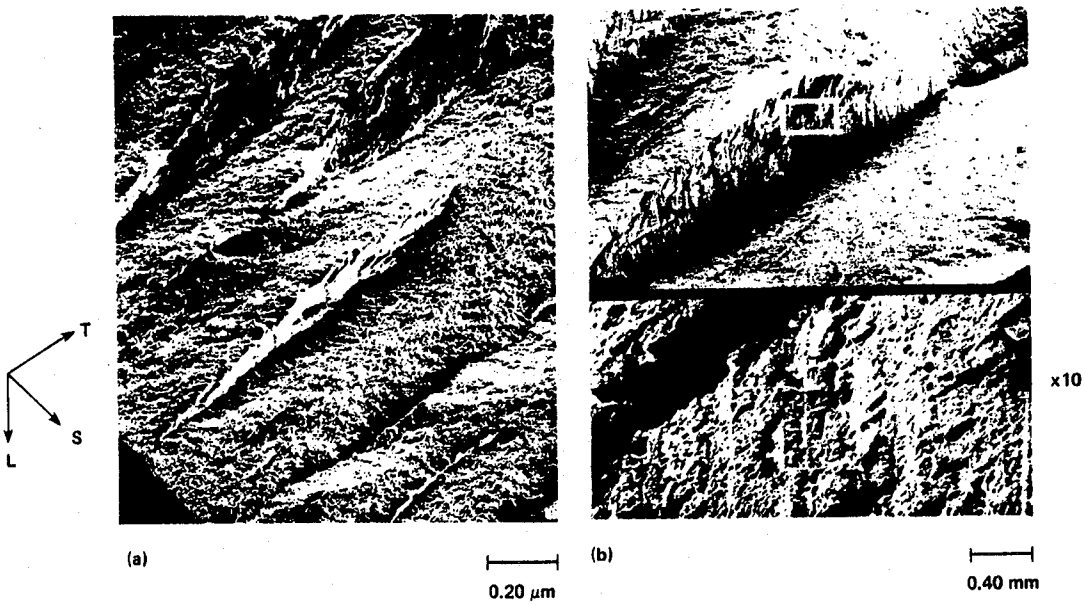

Fig. 24. Fatigue fracture surface of P/M Al-Li-Cu L-T oriented, CT specimen (ΔK = 12.5 MPa-$m^{1/2}$/dray FCGR conditions) (a) secondary crack ridges with S-L orientation, (b) fracture morphology on secondary crack plane.

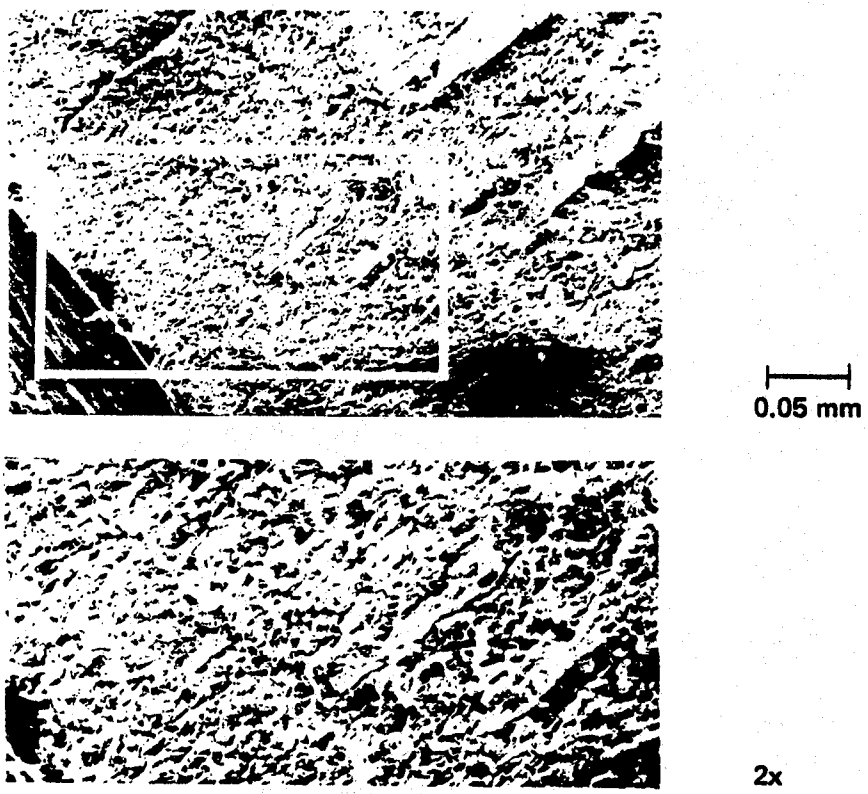

Fig. 25. Fatigue fracture surface of Al-Li-Cu (L-T) oriented CT specimen depicting fracture morphology characteristic of intermediate ΔK/wet FCGR conditions (a) initial crack growth region and (b) close-up of same.

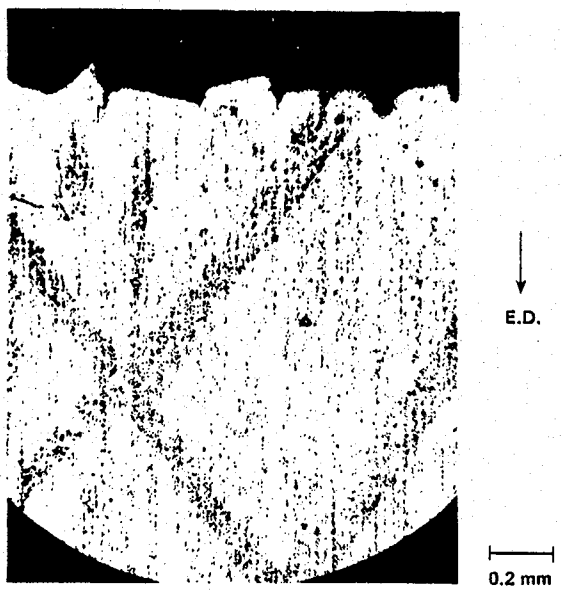

Fig. 26. Secondary cracking along stringer particles in transverse section of L-T oriented CT specimen of P/M Al-Li-Cu from FCGR study (a/w = 0.36/polished and etched in Keller's reagent).

similar to that observed in the base alloy, was observed; it is shown in Figure 27. Shear-deformation bands, similar to those observed in the base alloy, were not detected in any of the fatigue-tested magnesium-bearing alloy specimens.

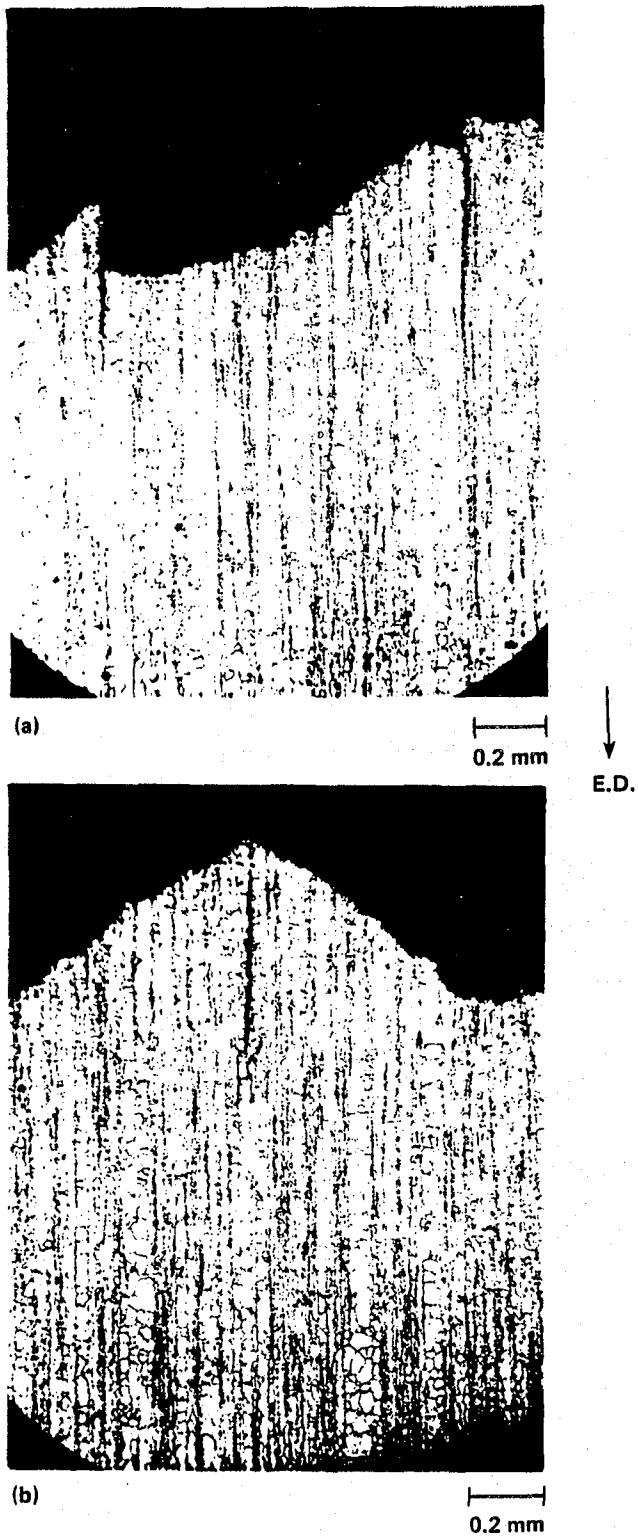

Fig. 27. Secondary cracks (S-L oriented) along stringer particles in transverse section of P/M Al-Li-Cu-Mg, L-T oriented, CT specimen (a) at a/w = 0.32 position, (b) at a/w = 0.54 position.

Discussion

Alternate-Immersion Tests

Crack-initiation studies performed on tuning-fork specimens under alternate-immersion conditions suggest that the T-S-oriented X-2020 alloy and the L-S-oriented M/A Al-Li-Mg alloy are by far the most resistant of the six alloys investigated to degradation in a sodium-chloride-containing aqueous environment (Fig. 9). No obvious surface cracks developed in either alloy after long exposures, even under high applied stresses (Figs. 6 and 7). The most susceptible alloy was found to be the T-S-oriented ingot AA7475 alloy (Fig. 9). The apparent threshold stress (the asymptote of the lower-limit curve of Fig. 8 at long times) of 275 MPa (40 ksi) is consistent with stress-corrosion classification data presented in ASTM Standard G64 (Table II, p. 1034). The three remaining alloys appear comparable to each other in terms of environmental degradation, and they are about midway between the two extremes. Additionally, no evidence was found to suggest any systematic difference between the degrading influence of either an aqueous 3.5% NaCl environment or a synthetic sea water environment. For the two P/M Al-Li-Cu alloys, longer aging times correlate with longer life and thus higher stress-corrosion resistance.

In the alternate-immersion tests, crack initiation and crack propagation both can play a role in determining the life of the specimen. The fraction of life spent in crack propagation is dependent on the value of the critical mode I stress-intensity factor for unstable, rapid fracture, K_{IC}. For low values of K_{IC}, initiation of a sharp flaw may be sufficient to meet the critical condition for rapid fracture, whereas if the fracture toughness is large, extensive stable crack growth may occur, and a major portion of life would be involved in crack propagation. In the case of the M/A and P/M Al-Li alloys, rather low fracture toughnesses of from 8 to 10 MPa-$m^{1/2}$ are typical (Table II). Thus, the corresponding critical flaw size for the alternate-immersion specimens are small; no greater than 0.38 mm for typical applied stresses. The longer secondary cracks observed in the failed P/M Al-Li-Cu specimens (Fig. 11) are consistent with the estimated critical flaw size. Thus, the life of the tuning-fork specimens under alternate-immersion conditions is dominated by crack-initiation events.

Constant-Immersion Tests

Crack Initiation. Constant-immersion data for P/M Al-Li-Cu alloy tuning-fork specimens tested under potentiostatic control indicate that crack initiation is clearly influenced by the electrochemical conditions. The failure time of similarly stressed P/M Al-Li-Cu specimens tested under anodic passivation conditions in deaerated 3.5% NaCl solution is at least 10 times longer than that observed in the alternate-immersion (free corrosion in aerated 3.5% NaCl solution) tests. Similar behavior is noted for the P/M Al-Li-Cu-Mg alloy; an approximate order-of-magnitude increase in failure time occurred for a test conducted under anodic passivation conditions. A common mode of pit formation and crack initiation was found. These data demonstrate that polarization methods can be used to control crack-initiation events in Al-Li-Cu alloys and thus allow systematic investigation of this phenomenon.

The failure of the magnesium-bearing alloy specimen tested under cathodic polarization conditions was unexpected. However, the mode of failure is unknown because excessive cell current upon specimen fracture made post-test examination impossible. Further data are required to characterize time-dependent fracture of P/M Al-Li-Cu alloys under cathodic polarization conditions.

It is interesting to contrast the slow-strain-rate test results for the P/M Al-Li-Cu alloy with the constant-immersion data for the tuning-fork specimens. Both tests were conducted under potentiostatic control within the passive film-formation region. The tests differ, however, in that the tuning-fork specimens were maintained at some high applied stress, and the specimens in the slow-strain-rate test were pulled to failure at some constant-displacement rate. Even though constant-immersion exposures of P/M Al-Li-Cu tuning-fork specimens ran to 2000 hr, fracture did not occur. However, the maximum duration for a slow-strain-rate test in this investigation was about 18 hr, and a definite environmental degradation was observed (Fig. 12). Localized pitting along the stringer particles occurred, and some associated intergranular cracking was observed (2). However, after 2000 hr of constant-immersion exposure, relatively mild pitting and no detectable intergranular cracking was observed in the tuning-fork specimens. The importance of deformation (or perhaps a sustained deformation rate) in the environmental degradation of P/M Al-Li-Cu in sodium chloride solution is demonstrated by these data.

There is metallographic evidence that the environmental degradation mechanism operative in the slow-strain-rate testing of the P/M Al-Li-Cu alloy is different from that observed in the alternate- and constant-immersion testing of tuning-fork specimens. Intergranular cracking associated with stringer particle pits was detected in each instance. However, in the slow-strain-rate tests, the extent of intergranular cracking was much less than the critical flaw size for rapid, unstable crack growth in these materials (2). Failure of the P/M tuning-fork specimens could always be predicted on the basis of the deepest intergranular crack and the known fracture toughness. Thus, some alternative mechanism of crack extension is required to explain the reduced tensile ductility observed in the slow-strain-rate test (Fig. 12). The requisite mechanism must exhibit relatively rapid kinetics and be electrochemically select; the possible role of hydrogen has been suggested (2).

Crack Propagation. Although crack initiation in 3.5% NaCl solution occurs readily in the P/M Al-Li-Cu alloys, crack propagation is difficult. This was confirmed in the constant-immersion testing of S-L-oriented DCB specimens bolt-loaded to a fixed displacement and of L-S-oriented four-point bend specimens fatigue-loaded at high mean stress. In the case of the DCB specimens immersed 159 days and loaded to within 10% of the known fracture toughness, slow crack extension was observed (Table IV). However, subsequent metallography and fractography revealed the crack extension to occur by a mechanical-tearing and localized crevice-corrosion mechanism. Thus, the apparent K_{ISCC} value does not represent a true stress-corrosion threshold. In the L-S-oriented four-point bend specimens fatigue-loaded at a high mean stress ($R \sim 0.95$) and at a maximum stress-intensity factor approaching the respective fracture toughness of the alloys, measurable crack extension did not occur (Table V); instead, the crack-tip blunted owing to crevice corrosion (Fig. 19).

Analysis of exposed DCB specimens confirmed the presence of localized intergranular corrosion (Figs. 14-17). The intergranular attack is more severe in the magnesium-bearing alloy (Fig. 17 versus Fig. 14); but in both P/M Al-Li-Cu alloys, the intergranular corrosion occurs in heavily deformed material such as that adjacent to the machined notch (Fig. 15a) and in the wake of the plastic zone of the fatigue precrack (Figs. 14 and 17). The intergranular attack is less extensive at the crack-tip in the region of intense stress localization (Figs. 15b and 6) and intergranular corrosion did not occur far from the crack crevice.

Preferential corrosion in regions of high deformation history is clearly indicated in Figure 14 where intergranular corrosion of the base alloy decorates shear-deformation bands formed during fatigue precracking. Accelerated corrosion of the highly strained shear-deformation band is not altogether unexpected, for the strain energy necessary to activate corrosion would be high in these regions. However, pitting and intergranular cracking extends from these bands along the oxide stringer particles in regions where the stress is greatly reduced from conditions at the crack-tip. Clearly, stress is not the primary variable driving the intergranular corrosion and crack mode.

The preference of intergranular attack for regions of high deformation history rather than regions of high stress intensity is also demonstrated in analysis of the four-point bend specimens. Localized pitting and intergranular corrosion occur in the material adjacent the machined notch (Figs. 18a and 19a) and in the material affected by passage of the fatigue precrack (Figs. 18b and 19b). The pitting occurs along the stringers of oxide particles that are oriented perpendicular to the main crack plane in these L-S-oriented specimens (Figs. 16 and 17).

From the above observations, it is apparent that deformation is a necessary requirement for the intergranular corrosion process. It is rationalized that deformation results in semicontinuous regions of microcracking and fracture along oxide stringer particles. In this manner, electrochemically active particles become exposed to the aqueous NaCl electrolyte or electrochemical conditions within the microcrack regions adjust to promote accelerated intergranular attack. Support for the latter hypothesis is present in the diversity of "external" electrochemical conditions in which a common mode of intergranular corrosion was observed in the P/M Al-Li-Cu alloys. Intergranular corrosion occurred at the free corrosion-potential in both alternate-immersion and constant-immersion tests, and in deaerated solution under a range of noble potentials for both smooth and flawed specimens.

The P/M Al-Li-Cu alloys are sensitive to the aqueous 3.5% NaCl environment under conditions of fatigue at low mean stress (Figs. 20-22). For the T-L orientation, in which the crack plane is parallel to the stringer particles, environmental sensitivity is observed for both the base and magnesium-bearing alloys (Fig. 22). Fatigue-crack-growth rate increases by a factor of 5 for aqueous NaCl exposure with respect to dry conditions, and this is the maximum effect observed under the parameters of this investigation. For the L-T orientation, in which the crack plane is perpendicular to the stringer particles, the fatigue-crack-growth rate is less sensitive to aqueous NaCl exposure; the magnesium-bearing alloy appears relatively insensitive (Fig. 21). Alternatively, however, the magnesium-bearing alloy may be more sensitive to environment than the base alloy, and moisture within the laboratory air may be sufficient to promote accelerated crack growth. Controlled humidity tests or tests in inert-gas or vacuum environments are required to complete the assessment of environmental influence.

A characteristic of the fatigue-crack growth rate versus stress-intensity factor range behavior of the P/M Al-Li-Cu alloy is the transition in shape of the trend curve at $\Delta K \sim 10$ MPa-$m^{1/2}$ (Fig. 20). This transition correlates with the reported transition in fracture morphology (Figs. 23 and 24). The fatigue-crack growth rate at ΔK values above the transition is retarded with respect to behavior below the transition. Fractographic data show that a tortuous three-dimensional crack path is created for $\Delta K > 10$ MPa-$m^{1/2}$ and that below this value, a more planar crack path is followed (Fig. 23). It is postulated that the higher energy requirement for the tortuous crack path results in retardation of the crack-growth rate above the transition.

The transition in fatigue-crack growth behavior may be an interactive effect of both stress state and environment. Since no evidence of intergranular cracking similar to that observed in the other tests of this investigation was found, environment-sensitivity of the P/M Al-Li-Cu alloys under fatigue at low mean stress is thought to be an interactive corrosion-fatigue process rather than a stress-corrosion assisted, crack-growth phenomenon.

Conclusions

Relative Stress-Corrosion Susceptibility of Al-Li Alloys

1) Alternate-immersion data demonstrate that a) time-dependent fracture can occur in Al-Li alloys exposed to an aqueous 3.5% NaCl environment and b) the stress-corrosion susceptibility is composition dependent.

2) Alloy X-2020 and mechanically alloyed Al-Li-Mg appear very resistant to stress corrosion.

3) The lower-limit threshold stress to cause fracture in the most susceptible Al-Li alloy (P/M Al-Li-Cu-Mg) was approximately 355 MPa (51.5 ksi); this value is consistent with reasonable stress-corrosion resistance.

The Stress-Corrosion Behavior of P/M Al-Li-Cu Alloys

1) P/M Al-Li-Cu alloys are susceptible to intergranular crack initiation in aqueous sodium chloride environments, but resistant to sustained subcritical crack growth for stress intensity factors up to 15 MPa-$m^{1/2}$.

2) At values approaching the fracture toughness, a slow crack-extension mechanism involving both localized corrosion and mechanical tearing is active. The ability to evaluate fully electrochemical and mechanical stress state conditions which may support classic stress-corrosion cracking of these alloys will require availability of more isotropically tough material.

3) A distinct ductility loss occurs in the slow-strain-rate test under anodic polarization conditions. However, the active degradation mechanism is different from the intergranular process operative in the alternate- and constant-immersion tests. For this reason, the slow-strain-rate test cannot be used to predict service stress-corrosion performance of the alloys.

4) Environmental sensitivity is also observed under conditions of fatigue at low mean stress. The apparent mechanism is corrosion-fatigue and it is orientation-dependent.

5) Pitting along oxide stringer particles and subsequent intergranular corrosion were observed for a variety of electrochemical conditions and for both constant and cyclic straining. This localized corrosion mechanism was active both at free surfaces and within crack crevices.

6) Tensile stress is a requirement for pitting and intergranular attack. However, these phenomena were associated more with regions of intense deformation than with regions of high stress intensity. The presence of intergranular corrosion in regions of low applied stress suggests that the intergranular corrosion may be dissolution-controlled.

7) Intergranular corrosion starts at active pitting sites correlated to oxide particles strung along the extrusion direction of the alloys. It is hypothesized that active phases or particles are present at high density along the extrusion direction and that these particles become fragmented by

prior or concurrent deformation. Rapid dissolution occurs, altering local electrochemistry within crack crevices, thus promoting intergranular corrosion.

8) The stringer oxide particles play a key role in determining the stress-corrosion behavior of the P/M Al-Li-Cu alloys in aqueous NaCl solution. Since the nature, size, and distribution of these particles may be influenced by process history and heat treatment, the stress-corrosion resistance of the alloys may be at least partially controlled.

Acknowledgments

The authors acknowledge NASA support of this research through Cooperative Agreement NCC2-155 with San Jose State University. In addition, NASA is acknowledged for providing coauthor Ray Galvin with materials research experience through a cooperative work study program with De Anza College of Cupertino, California.

References

1. P. S. Gilman, "The Physical Metallurgy of Mechanically Alloyed Dispersion Strengthened Al-Li-Mg and Al-Li-Cu Alloys," The Second International Conference on Aluminum-Lithium Alloys, T. H. Sanders, Jr. and E. A. Starke, Jr., eds., Conference Proceedings, The Metallurgical Society of AIME, 1983.

2. P. P. Pizzo, R. P. Galvin, and H. G. Nelson, "Utilizing Various Test Methods to Study the Stress-Corrosion Behavior of Al-Li-Cu Alloys," ASTM STP821, E. N. Pugh and G. M. Ugiansky, eds., American Society for Testing and Materials, 1982.

1. Report No.	2. Government Accession No.	3. Recipient's Catalog No.
NASA TM 85853		

4. Title and Subtitle	5. Report Date
STRESS-CORROSION BEHAVIOR OF ALUMINUM-LITHIUM ALLOYS IN AQUEOUS SALT ENVIRONMENTS	October 1983
	6. Performing Organization Code
7. Author(s)	8. Performing Organization Report No.
P. P. Pizzo,* R. P. Galvin and Howard G. Nelson	A-9499
	10. Work Unit No. T-4241
9. Performing Organization Name and Address	11. Contract or Grant No.
Ames Research Center, Moffett Field, CA 94035, *Department of Materials Engineering, San Jose State University, San Jose, CA 95192	
	13. Type of Report and Period Covered Technical Memorandum
12. Sponsoring Agency Name and Address	14. Sponsoring Agency Code
National Aeronautics and Space Administration Washington, D.C. 20546	505-33-21

15. Supplementary Notes

Point of Contact: Patrick P. Pizzo, Associate Professor, Department of Materials Engineering, San Jose State University, San Jose, CA 95192 (408) 277-2436 or (408) 277-2446

16. Abstract

The stress-corrosion susceptibility of two powder-metallurgy (P/M) alloys, Al-Li-Cu and Al-Li-Cu-Mg; two mechanically attrited (M/A) alloys, Al-Li-Cu and Al-Li-Mg; and two wrought, ingot alloys, X-2020 and AA7475, are compared. Time-dependent fracture in an aqueous sodium chloride environment under alternate-immersion condition was found to vary significantly between alloys. The stress-corrosion behavior of the two powder-metallurgy processed alloys was studied in detail under conditions of crack initiation, static crack growth, and fatigue-crack growth. A variety of stress-corrosion tests were performed including smooth-surface, time-to-failure tests; potentiostatic tests on smooth surfaces exposed to constant applied strain rates; and fracture-mechanics-type tests under static and cyclic loads. Both alloys show surface pitting and subsequent intergranular corrosion. Pitting is more severe in the magnesium-bearing alloy and is associated with stringer particles strung along the extrusion direction as a result of P/M processing. Both alloys were found to resist stress-corrosion crack extension at low and moderate stress intensities under conditions of both static and cyclic (high-mean stress) loading. Fatigue-crack growth at low-mean stress is shown to be somewhat environment- and microstructure-sensitive. These results are supported by relevant fractographic and metallographic observations and are discussed in terms of the potentially active stress-corrosion processes.

17. Key Words (Suggested by Author(s))	18. Distribution Statement
Aluminum-lithium alloys; Powder-metallurgy processing; Stress corrosion; Intergranular corrosion; Fatigue crack growth; Aqueous salt exposure; Slow strain-rate	Unlimited Subject Category: 26

19. Security Classif. (of this report)	20. Security Classif. (of this page)	21. No. of Pages	22. Price*
Unclassified	Unclassified	33	A02

*For sale by the National Technical Information Service, Springfield, Virginia 22161